

1 **Microbiome diversity protects against pathogens by nutrient blocking**

2 Frances Spragge^{1,2+} and Erik Bakkeren^{1,2+}, Martin T. Jahn^{1,2}, Elizete B. N. Araujo³, Claire F. Pearson³,

3 Xuedan Wang^{1,2}, Louise Pankhurst^{1,2}, Olivier Cunrath^{4*} and Kevin R. Foster^{1,2*}

4 ⁺These authors contributed equally to this work

5 *Corresponding authors: kevin.foster@biology.ox.ac.uk; olivier.cunrath@unistra.fr

6 1. Department of Biology, University of Oxford, Oxford, UK

7 2. Department of Biochemistry, University of Oxford, UK

8 3. Kennedy Institute of Rheumatology, University of Oxford, UK

9 4. CNRS, UMR7242, Biotechnology and cell signaling, University of Strasbourg, Illkirch, France

10 **Abstract**

11 The human gut microbiome plays an important role in resisting colonization of the host by pathogens,
12 but we lack the ability to predict which communities will be protective. We studied how human gut
13 bacteria influence colonization of two major bacterial pathogens, both *in vitro* and in gnotobiotic
14 mice. While single species alone had negligible effects, colonization resistance greatly increased with
15 community diversity. Moreover, this community-level resistance rested critically upon certain species
16 being present. We explain these ecological patterns via the collective ability of resistant communities
17 to consume nutrients that overlap with those used by the pathogen. Further, we apply our findings to
18 successfully predict communities that resist a novel target strain. Our work provides a reason why
19 microbiome diversity is beneficial and suggests a route for the rational design of pathogen-resistant
20 communities.

21

22 **One sentence summary**

23 Diverse communities of gut bacteria collectively limit pathogen colonization by blocking nutrient
24 access.

25 **Introduction**

26 The human gut is home to diverse bacterial species collectively known as the gut microbiota. A major
27 health benefit provided by the gut microbiota is protection against pathogen colonization and
28 subsequent infection; a phenomenon known as colonization resistance (1). The ability of the
29 microbiota to protect against numerous enteric pathogens is well-documented, with evidence that
30 particular species within the microbiota play a more important role than others (2-9). The ways that
31 colonization resistance can arise include competition for nutrients and space, direct antagonism by
32 toxins and other harmful compounds, and promoting host immunity against pathogens (1, 10, 11).

33 While the importance of the microbiota for colonization resistance is clear, however, we currently
34 lack the principles needed to predict, *a priori*, which microbiota species will be effective against a
35 given pathogen. A key challenge is the ecological complexity of the gut. The gut microbiome is a
36 diverse ecological system with many individual species that all have the potential to play a role in
37 colonization resistance. Moreover, these constituent species can also affect each other and interact
38 ecologically in ways that are critical for colonization resistance (12-16). This combination of species
39 diversity and the potential for ecological interactions makes colonization resistance a challenging
40 phenotype to understand (17).

41 Here we approached the question of mechanisms of colonization resistance from the
42 perspective of the underlying ecological principles. To do this, we studied colonization resistance
43 provided by a range of human gut bacteria, both alone and in combinations. We performed all
44 experiments in parallel using two species of pathogen, which are both on the WHO priority list:
45 *Klebsiella pneumoniae* and *Salmonella enterica* Serovar Typhimurium (18). Both are members of the
46 Enterobacteriaceae found in the human gut microbiome but they have very different lifestyles. *S.*
47 Typhimurium causes acute infection and gastroenteritis (19, 20). By contrast, *K. pneumoniae* is a
48 nosocomial, opportunistic pathogen that rarely causes disease in the gut itself, but gut colonization is a
49 major risk factor for antimicrobial resistance associated infections elsewhere in the body (21).

50 Despite these differences, we have identified common principles that underlie colonization resistance
51 to both species. Ecological diversity is important for colonization resistance *in vitro* and in gnotobiotic
52 mice. Moreover, we found that colonization resistance is an ecologically complex trait, whereby the
53 ability of one species to provide colonization resistance can depend entirely upon the presence of
54 other species (22). Despite the complexity, we find that these ecological patterns are explained by a
55 simple underlying principle, the collective ability of certain communities to consume nutrients and
56 block pathogen growth. Further, we have shown that this principle offers a way to identify sets of
57 bacterial species that will collectively limit the growth of a particular pathogen.

58 **Results**

59 **Single species offer little protection in competition with pathogens**

60 Individual members of the microbiota can promote colonization resistance in various contexts (2-8),
61 which suggests that some species are more important for colonization resistance than others. To
62 systematically assess this variability, we screened a diverse set of 100 human gut symbionts (**Table**
63 **S1; also see Methods**) for their ability to limit pathogen growth. Competition in the gut occurs both at
64 the point a pathogen enters the gut and when a pathogen becomes established (23, 24). We designed
65 two co-culture assays to reflect these two aspects of competition in the mammalian gut (**Fig. 1a**). In
66 the first assay (ecological invasion assay), we pre-grew the symbiont alone in standard anaerobic
67 media (modified Gifu anaerobic media; mGAM) buffered to human colonic pH before adding the
68 pathogen. In the second assay (competition assay), we inoculated this media with an equal ratio of
69 symbiont to pathogen, which is designed to capture competition once a pathogen has established itself
70 in the gut.

71 To assess pathogen growth, we built luminescent strains of *K. pneumoniae* and *S.*
72 Typhimurium and compared luminescence when grown in monoculture and when grown in co-culture
73 with each symbiont. With this assay system, we could rank the strains based on their abilities to limit
74 pathogen growth in both the invasion and competition assays (**Fig. 1b-c, S1**). From this ranking, we
75 took the top ten best-performing non-pathogenic symbiont species in the screen (Methods; shown in

76 orange in **Fig. S1e-f; Table S1**) and subjected them to a more stringent test of colonization resistance
77 designed to capture both phases of competition in the gut in one assay (extended competition assay,
78 **Fig. 1d**). Here, the pathogen is first introduced into a pre-grown culture of a given symbiont strain and
79 then, after 24 hours, the mixture is passaged into fresh media and allowed to grow for 24 hours,
80 whereafter pathogen abundance is assessed via flow cytometry (**Fig. 1d**). Despite choosing the best-
81 ranked species from the luminescence screen, all symbionts performed poorly under extended
82 competition, with the majority offering no discernible colonization resistance (**Fig. 1e-f**). The best
83 performer was *Escherichia coli*, a known competitor of *S. Typhimurium*, and also a member of the
84 Enterobacteriaceae, but even here the protection offered was very limited with the pathogens still able
85 to reach $10^8 - 10^9$ cells/ml.

86 The outcome of the assay differed greatly when we pooled all ten strains together (**Fig. 1e-f**).
87 Now, the final abundance of both pathogens was strongly suppressed by over three orders of
88 magnitude for *K. pneumoniae* and about two orders of magnitude for *S. Typhimurium*. By contrast, a
89 community made up of the ten worst-performing strains from the luminescence screen (shown in blue
90 in **Fig. S1e-f**) provided little or no colonization resistance (**Fig. 1e-f**). These results, therefore, suggest
91 that strain identity is important for colonization resistance only in the context of a diverse community.

92

93 **Ecological diversity and complexity drive colonization resistance *in vitro***

94 Our results indicated that microbiota diversity is important for colonization resistance. This finding
95 fits well with the general idea that microbial diversity is beneficial for microbiome functioning,
96 whereas a loss of diversity, or dysbiosis, can be associated with poor health and disease (25-27).
97 While the potential benefits of diversity are clear, cause and effect can be confounded in observational
98 studies (28). To systematically test the role of diversity in colonization resistance, we randomly
99 selected communities of increasing diversity from the best ranked 10 strains and competed them
100 against the pathogens in the extended competition assay. To further evaluate the importance of
101 diversity, we also assembled a community of 50 non-pathogenic symbiont species from the strains in

102 our initial luminescence screen (see Methods). These data indicated a relationship between diversity
103 and colonization resistance. However, we also saw a large variation in colonization resistance across
104 the communities that differed in their composition of two, three and five species. Visual inspection of
105 the data (**Fig. 2c-d**) suggested that a large component of this variability was driven by the composition
106 of the communities.

107 One species that appeared to be important for outcomes was *E. coli*. To explore this finding,
108 we randomly selected additional *E. coli*-containing communities and again evaluated colonization
109 resistance (**Fig. 2c-d**). We also performed drop-out experiments, where we made up the 10 and 50
110 species communities without *E. coli* (**Fig. 2c-d**). These data revealed a strong and clear monotonic
111 increase in colonization resistance as species diversity increases (**Fig. 2c-d, green circles**), but this
112 relationship is much weaker or disappears entirely in the absence of *E. coli* (**Fig. S2a-b**). In ecological
113 terms, these data show that colonization resistance rests upon a strong higher-order effect involving
114 other community members and *E. coli* (22). By higher-order effects here, we mean cases where the
115 effect of one species on another is changed by the presence of a third-party species in a community
116 (22). That is, while *E. coli* alone or the rest of the community alone each have little impact on
117 pathogen growth, together they have a strong effect on pathogen growth. Such higher-order effects are
118 considered important in ecology as they imply context dependence, which can make a system difficult
119 to understand and predict (22, 29-32). Another way to illustrate the effect of diversity on colonization
120 resistance is to compare our data to a simple null model. Consider, for example, a model where each
121 additional species proportionally improves colonization resistance to the pathogen. Specifically, we
122 can compare our experimental data for *E. coli* containing communities to a null model where
123 pathogen abundance scales according to $1/n$, where n is the number of species present. This analysis
124 shows that the deviation from such a null model increases as diversity increases, where colonization
125 resistance is again greater than expected for diverse communities (**Fig. S3**).

126 We also asked whether the role of *E. coli* within communities was a strain-specific effect. We
127 replaced *E. coli* strain IA11, identified in our screen, by each of four other *E. coli* strains historically
128 isolated from the human gut (33-35). The effect of *E. coli* was similar when *E. coli* IA11 was

129 substituted by most *E. coli* strains (**Fig. 2e-f**), which indicates that the higher-order effect involving *E.*
130 *coli* is a general property of closely-related strains.

131 Further inspection of the data pointed to other species that were important for colonization
132 resistance in diverse communities. In *E. coli* containing communities, the presence of *Bifidobacterium*
133 *breve* appeared to be important in excluding *K. pneumoniae* (**Fig. S4a**), and *Lacrimispora*
134 *saccharolyticum* and *Phocaeicola vulgatus* in the exclusion of *S. Typhimurium* (**Fig. S4b**). We
135 confirmed these patterns through a series of systematic drop-out experiments (**Fig. S4c-d**). However,
136 it was still possible to achieve equivalent colonization resistance in more diverse communities that
137 lack these species (**Fig. S4c-d**), which again points to the underlying benefits of a diverse microbiota.

138

139 **Ecological diversity and complexity also drive colonization resistance *in vivo***

140 To validate our *in vitro* methods, we tested the ability of symbiont communities to resist pathogen
141 colonization in gnotobiotic mice (**Fig. 3a**). Germ-free mice were colonized with symbiont
142 communities differing in diversity, and the presence or absence of *E. coli*. Successful colonization by
143 *S. Typhimurium* causes an acute infection and massive gut inflammation, which is a major
144 confounding effect for studying the effects of community composition on pathogen growth. Animals
145 with a less protective microbiota can rapidly succumb to the infection, such that one cannot follow
146 ecological dynamics over time in a comparable way across treatments. We, therefore, chose to use an
147 avirulent variant of *S. Typhimurium* to eliminate the effect of gut inflammation on pathogen and host,
148 where one can use pathogen abundance as a measure of disease risk (19, 36, 37). We introduced
149 communities across the same range of diversities as before but, in contrast to *in vitro* assays, not all
150 symbiont species will reliably colonize germ-free mice (38). Therefore, we used metagenomic
151 sequencing to confirm that introducing a higher diversity community to the mice did indeed result in a
152 higher diversity of strains colonizing the gut as measured by two metrics of alpha diversity, and to
153 identify the relative abundance of all members (**Fig. 3b-c, S5**).

154 These experiments revealed that, as observed *in vitro*, microbiome diversity is negatively
155 correlated with pathogen abundance in feces for both pathogens (compare 10 vs 50-member
156 communities; **Fig. 3d-e**; **Fig. S6**). Moreover, drop-out experiments revealed again the importance of
157 the combination of *E. coli* and other community members for colonization resistance (**Fig. 3d-e**). We
158 also observe that higher diversities are needed for efficient colonization resistance in the mammalian
159 gut than in our *in vitro* assays, which is likely to be explained by the higher degree of environmental
160 and spatial heterogeneity in the gut compared to a test tube. Nevertheless, the key patterns remain the
161 same between the gnotobiotic mouse experiments and our *in vitro* assays. Both ecological diversity
162 and higher-order interactions are important for colonization resistance to both pathogens. As before,
163 we saw a strong deviation from a simple null model of ecological competition at high levels of
164 diversity (**Fig. S3**). In addition to showing the generality of these patterns, this fit between the *in vitro*
165 and *in vivo* methods validates our extended competition assay as an approach to interrogate the
166 ecology of colonization resistance.

167

168 **A simple principle explains the roles of diversity and complexity in colonization resistance**

169 The discovery of such higher-order effects in colonization resistance indicates that colonization
170 resistance is an ecologically complex trait (22), which can be challenging to work with owing to high
171 levels of context dependence (17, 22, 29, 30). Nevertheless, we sought to understand the mechanisms
172 underpinning colonization resistance by returning to our *in vitro* data gathered from large numbers of
173 different communities. The genomic data enabled us to assess functional similarity between symbiont
174 communities and pathogens from overlap in protein compositions. Specifically, we calculated the
175 percentage of all protein families carried by a pathogen that were also present in each community
176 investigated (see Methods). We reasoned that this measure of functional similarity may map to niche
177 overlap and, therefore, the strength of ecological competition between symbionts and pathogens. We
178 first confirmed that the number of encoded protein families covered by our experimental communities
179 increases proportionally with the number of added strains (**Fig. S7**). Permutation analyses also

180 confirmed that the randomly selected communities we have studied experimentally are a good
181 representation of all possible communities that we could have studied (**Fig. S8**).

182 The potential importance of protein family overlap was already clear from the effects of *E.*
183 *coli* in our experimental data (**Figs. 2-3**). *E. coli* is in the same family of bacteria as *K. pneumoniae*
184 and *S. Typhimurium* and can be seen to contribute greatly to the overlap in the protein families carried
185 by a given community and either of the pathogens in our experimental communities (**Fig. S9a-d**).
186 However, by taking only the communities that contain *E. coli* to control for this effect, we also see a
187 strong correlation between a community's protein family overlap with the pathogen and its
188 colonization resistance in our *in vitro* assays (**Fig. 4a-b; Fig. S9**). In other words, if the symbiont
189 strain or community encoded many of the same (or similar) proteins as the pathogen, it provides better
190 colonization resistance. The same analysis for communities that lack *E. coli* is not informative as
191 colonization resistance is consistently so low across all communities (**Fig. 2**).

192 Altogether, our genomic analysis suggests that communities that overlap highly with the
193 pathogens in encoded functions provide the best colonization resistance. These analyses support our
194 hypothesis that niche overlap is important for our observed ecological patterns in colonization
195 resistance. One of the key drivers of niche overlap is resource competition (39, 40), which is a known
196 contributor to colonization resistance to *K. pneumoniae* and *S. Typhimurium* (12, 13). We, therefore,
197 explored the role of nutrient competition by generating metabolic profiles for the two sets of 10 key
198 symbiont species identified in the original screen against each pathogen (**Fig. 1**) using AN Biolog
199 MicroPlates that profile the metabolic activity of each strain on 95 carbon sources (**Fig. S10**). Note
200 that to cover the two sets of 10 species, we only profiled 16 strains in practice because there were
201 some parallels between the two sets of top-ranked strains in the luminescence screen. We first
202 established that there was a strong positive association between the protein family (genomic) and
203 metabolic (Biolog) overlap of communities with the pathogens (**Fig. S11**). We then assessed the
204 ability of metabolic overlap to predict colonization resistance (**Fig. 4c-d**). Colonization resistance was
205 only observed once communities shared sufficiently high overlap in their carbon source utilisation
206 profile with a pathogen. Moreover, communities with the greatest metabolic overlap with a pathogen

207 provided the greatest colonization resistance. An important observation from these data is that it is not
208 diversity *per se* that predicts colonization resistance, it is the overlap between the pathogen and the
209 communities. This pattern is made clear by the observation that communities of different diversities,
210 but the same overlap, appear proximally in the plots (neighbouring points of different color in **Fig. 4c-**
211 **d**).

212 Overall, our data point to the importance of nutrient competition, and specifically nutrient use
213 overlap between a community and a pathogen, as an explanation for the patterns we observe in
214 colonization resistance. To further support this conclusion, we performed experiments where the
215 pathogens were grown in cell-free (spent) media collected from different communities, which
216 excluded cell-cell contact mechanisms as explanations for colonization resistance. Growing the
217 pathogen in the spent media of *E. coli* and the 10 species communities recapitulated the patterns seen
218 in the competition experiments, consistent with the effect of nutrient competition (**Fig. S12**). As a
219 final test, we sought a nutrient that can be used by the pathogens only and used it to perform nutrient
220 supplementation experiments (**Fig. 4e-f**). We identified galactitol from the Biolog plates (**Fig. S10**).
221 The pathogens can use this sugar alcohol but it has the desirable property that it cannot be used by any
222 of the symbionts in our focal 10-species communities, except for *E. coli*. We engineered a strain of *E.*
223 *coli* that lacks the transporter for cell import (*E. coli gatABC* deletion mutant). By adding in galactitol
224 to our standard media, we found that colonization resistance in a diverse community is lost if the
225 pathogens can use the nutrient but *E. coli* cannot (**Fig. 4e-f**). However, colonization resistance is
226 restored when *E. coli* can use the nutrient. Further, if a pathogen is engineered so that it cannot use
227 galactitol (*S. Typhimurium gatABC* deletion mutant), colonization resistance is restored. These
228 outcomes are exactly as expected if nutrient competition is the cause of colonization resistance.

229 Our data show that the ability of a microbiota community to consume nutrients required by a
230 pathogen for growth underlies the colonization resistance we observe. Importantly, the nutrient
231 blocking effect is a property of the whole community rather than any one species alone. That
232 colonization resistance is a community-level trait explains the importance of the ecological diversity,
233 and complexity (22) we observed in our experiments. Despite considerable genomic and metabolic

234 overlap with the pathogens, a species like *E. coli* cannot alone block enough nutrients to provide
235 colonization resistance. It is only in combination with other species, that *E. coli* becomes effective at
236 limiting pathogen growth.

237

238 **Nutrient blocking can identify protective communities**

239 Our experiments indicate that colonization resistance is an ecologically complex trait, but that this
240 complexity can be understood and predicted via a simple underlying principle. As an additional test of
241 these findings, we used the nutrient blocking to predict community compositions that provide
242 colonization resistance to a bacterial strain that was not present in our initial experiments. For this
243 test, we chose an antimicrobial resistant (AMR) clinical *E. coli* strain, which was isolated from the
244 urine of a patient. AMR *E. coli* strains are a major current target for alternatives to antibiotics because
245 members of this species have recently been found to be responsible for the most AMR-associated
246 deaths of any bacterial species (41).

247 We first analysed the AMR *E. coli* isolate on AN Biolog MicroPlates to assess its carbon
248 source utilisation and compared this to the top ranked strains from our initial luminescence screen
249 (**Fig. 1**). We reasoned that these top-ranked strains were a good place to start as *E. coli* is also a
250 member of the Enterobacteriaceae, like the two pathogens that were used to select the top-ranked
251 strains. As expected, the AMR *E. coli* had the greatest protein overlap with the symbiont *E. coli* in our
252 16 strains but, importantly, additional strains were predicted to be required to block nutrient
253 availability based on the overlap needed to suppress the two pathogens (**Fig. S13**). We next used the
254 Biolog data to computationally assemble all possible communities of one, two, three and five species
255 from the 16 strains and calculated their resource utilisation overlap with the AMR *E. coli* (**Fig. 5a**).
256 Again, in line with our findings, diversity improved the median resource utilisation overlap, but this
257 depended strongly on the presence of the symbiont *E. coli*.

258 The simplest test of the importance of nutrient blocking is to remove the symbiont *E. coli*
259 from a community and test the impact. Doing this for the community of all 16 strains confirmed the

260 importance of *E. coli* for colonization resistance (**Fig. 5b**). However, we also tested our ideas on
261 communities that contain *E. coli*. In these experiments we identified communities predicted to have
262 the highest and lowest overlap with the target strain at each diversity level, where communities were
263 randomly chosen if there were ties in rank. We then used our extended competition assay (**Fig. 1d**) to
264 test the ability of the AMR *E. coli* to invade the communities. As predicted by nutrient blocking, this
265 revealed that increasing diversity leads to increased colonization resistance and, critically, for each
266 diversity level, the community predicted to resist the AMR *E. coli* consistently performed better in
267 colonization resistance than the community predicted to do poorly (**Fig. 5b**). This result was clearest
268 for the two and three species communities. For the five species community, the best performing
269 community was only marginally better than the worst. We reasoned that this was because, in these
270 experiments, we are limited to choosing from 16 strains that were preselected for being relatively
271 good competitors to Enterobacteriaceae (**Fig. 1b-c, S1**).

272 To test the nutrient blocking principle more robustly we selected from a wider range of
273 possible strains from our set of 50 strains that we used in our *in vitro* and *in vivo* experiments (**Fig. 2-**
274 **3**). Most of these strains had not been characterised for their functioning in community-level
275 colonization resistance, other than in the 50 species treatment. We also used this set of experiments to
276 test the power of the nutrient blocking principle to predict colonization resistance based upon genomic
277 data alone. Rather than using the Biolog phenotypic assay, therefore, we returned to our measure of
278 protein family overlap, which calculated the overlap in all protein types between an invading strain
279 and different communities. To do this we only had to sequence the AMR *E. coli* clinical isolate
280 because all 50 other strains were sequenced. Using the same approach as for the Biolog predictions,
281 we then assembled communities *in silico* that all contained the symbiont *E. coli* strain and, in each
282 case, calculated their protein family overlap with the AMR *E. coli* (**Fig. 5c-d**). As before, we chose
283 communities with the lowest and highest overlap to the AMR *E. coli* across a range of diversities
284 (randomly choosing communities if there were ties in rank) and experimentally assessed colonization
285 resistance using the extended competition assay.

286 We again see the importance of community diversity in these experiments. Moreover, despite
287 using only genomic information and a much larger set of possible communities, we observed
288 improvement in colonization resistance from the worst to best communities at each diversity level
289 (**Fig. 5e**). Finally, we evaluated our ability to select highly and poorly performing communities by
290 assessing colonization resistance in additional five-species communities. Notably, at the five-species
291 level, more than 200,000 communities with *E. coli* can be assembled from 50 strains. We used our
292 algorithm to sample approximately 50,000 and, from these, we identified four additional community
293 compositions predicted to perform well and four predicted to perform poorly (to give five of each
294 class). In line with our predictions, the communities predicted to be colonization resistant showed a
295 median 100-fold reduction in the abundance of the AMR *E. coli* compared to those predicted to be
296 permissive (**Fig. 5f**).

297

298 **Discussion**

299 A key benefit of the microbiome is its ability to reduce the probability of infection via colonization
300 resistance (1, 2, 10, 42). Here we have used an ecological approach to understand the principles of
301 colonization resistance in the gut microbiome. By screening a collection of human gut symbionts, we
302 found that individual strains were unable to provide effective resistance to pathogens (**Fig. 1**), but that
303 colonization resistance increases monotonically with ecological diversity (**Fig. 2-3**). Our work,
304 therefore, supports the general hypothesis that a more diverse microbiome can carry health benefits
305 (28, 43-45). While much discussed, evidence for this hypothesis is typically based upon correlations
306 between microbiome diversity and health outcomes (28, 45, 46). Here, we provide experimental
307 evidence that microbiome diversity can provide health benefits via an increased ability to protect
308 against pathogens. Moreover, we explained this pattern in terms of the importance of the overlap
309 between the nutrient requirements of an invading pathogen and the resident community (**Fig. 4**).

310 We found that certain combinations of species display much greater colonization resistance
311 together than when alone. These non-additive effects mean that colonization resistance is formally a

312 complex ecological trait in the canon of ecology (22). Such effects are often assumed to imply a
313 complex network of interactions between species where, for example, one symbiont species affects a
314 second symbiont species and changes the way this second species interacts with a pathogen. However,
315 consideration of nutrient competition and particularly the level of overlap between a pathogen and
316 community revealed that much simpler processes explain the complexity we see. One species alone is
317 not sufficient to strongly impact pathogen growth, but rather a combination of species is required to
318 block nutrient access. Interestingly, the combinations of species that make colonization-resistant
319 communities are often very phylogenetically diverse. Generating resistant communities does not rest
320 upon simply finding closely related species to a given pathogen, in our case against
321 Enterobacteriaceae members. Instead, a mixture of gram-positive and gram-negative species is often
322 what performs best (**Fig. 5f, Table S7**). While both of our pathogens are members of the same family,
323 they have different life histories (19-21). *S. Typhimurium* is a specialist gut pathogen while *K.*
324 *pneumoniae* is an opportunistic pathogen that typically causes no pathology in the gut itself, instead
325 causing infections in other parts of the body. Consistent with this, we find it is consistently easier to
326 generate colonization resistance to *K. pneumoniae* than *S. Typhimurium*. Nevertheless, the importance
327 of ecological diversity and complexity is observed for both pathogens. We anticipate that the
328 importance of ecological diversity and the principle of nutrient blocking will apply generally, given
329 the widespread evidence that nutrient competition is important for diverse species in the microbiome,
330 including many other pathogens (9, 47-55).

331 By assembling a wide range of communities of defined compositions, we have been able to
332 establish links between ecological diversity, complexity and nutrient competition in colonization
333 resistance. However, a limitation of this approach is that we have focused on relatively low diversity
334 communities (up to 50 species). A question for the future is whether our findings will hold for the
335 higher levels of diversity that can naturally occur in the human microbiome. Consistent with our
336 findings, colonization risk with species like *K. pneumoniae* is increased after antibiotic treatment that
337 can lower species diversity in the microbiome (56). Nutrient competition is central to the patterns that
338 we have described here. Colonization resistance can develop via additional mechanisms, which

339 include toxin-mediated bacterial competition and effects via the host immune system (1, 10). Our
340 work does not exclude the potential importance of these additional mechanisms such as direct killing
341 of invading strains by members of the community, which can act in parallel to nutrient competition
342 (12, 13, 15, 39). Moreover, our predictions of resistant and permissive communities are not perfect
343 (e.g., high overlap communities in **Fig. 4c**; the outlier in **Fig. 5f**). However, it is notable that these
344 deviations are in the direction of a community being more resistant than expected. This suggests that
345 predictions based upon nutrient blocking may often be conservative with errors resulting in
346 communities performing better than expected whenever other mechanisms of colonization resistance
347 are at play.

348 Our work shows that colonization resistance is not the property of single microbiome species
349 but instead the collective property of multiple species. Specifically, we find that the effect of a given
350 symbiont species on a pathogen can be strongly dependent on whether other symbiont species are also
351 present to consume nutrients that the pathogen needs. This finding suggests that one can use the idea
352 of nutrient blocking to identify sets of microbiome species that will limit the growth of a target strain.
353 As a proof-of-principle, we tested this idea for an AMR *E. coli* strain, which revealed that species sets
354 can be successfully identified that collectively suppress an incoming strain (**Fig. 5**). Importantly, we
355 find that this can be done without specific information on available nutrients or the metabolism of the
356 species under study. Instead, a measure of genomic overlap can be used as a proxy for niche overlap
357 to assemble communities that perform nutrient blocking (**Fig. 5c-f**). The human microbiome is
358 dauntingly complex and has great potential for context-dependent effects. However, we found that
359 microbiome complexity can arise via simple underlying principles, which gives promise to the goal of
360 rationally designing microbiomes for better health.

361

362 **Materials and methods**

363 **Bacterial strains and plasmids** A full list of bacterial strains used in this study is provided in **Table**
364 **S1**. The plasmids used in this study are listed in **Table S2**. *Klebsiella pneumoniae* subsp. *pneumoniae*
365 purchased from DSMZ (stock number 30104) was used in all experiments containing *K. pneumoniae*.

366 *Salmonella enterica* serovar Typhimurium (strain SL1344 (57)) was used in all experiments containing
367 *S. Typhimurium*. The 100 strains were chosen for being abundant and/or important members of the
368 human gut microbiota that cover the key phylogenetic groups found in the human gut microbiota. In
369 addition, all are type strains, have had their genome sequenced (which we rely on for the protein family
370 analysis), and are known to be culturable in nutrient-rich, anaerobic medium (mGAM) (58, 59), so were
371 conducive to experimental work. Strains were kindly provided by Nassos Typas (EMBL Heidelberg,
372 Germany), or were ordered from the German Collection of Microorganisms, DSMZ or the American
373 Type Culture Collection (ATCC; *Staph. epidermidis*). The *Lactobacillus plantarum* strain was provided
374 by the Department of Food and Nutritional Sciences, University of Reading. *Klebsiella pneumoniae*
375 ATCC 700721 was provided by the Modernising Medical Microbiology research group, Nuffield
376 Department of Medicine, University of Oxford. *Escherichia coli* strains Z1331 and Z1269 were isolated
377 from the feces of two healthy human donors in Switzerland (33). The ampicillin-resistant AMR *E. coli*
378 strain is a urine clinical isolate provided by the Pathogen Bank at Nottingham University Hospitals NHS
379 Trust.

380 **Bacterial growth conditions** For engineering of *E. coli*, *K. pneumoniae*, or *S. Typhimurium*, strains
381 were grown aerobically in Lysogeny broth (LB; Fisher Scientific) with the appropriate antibiotics
382 (Table S1) at 37°C, shaking at 220 rpm. All symbionts were cultured under anaerobic conditions (5%
383 H₂, 5% CO₂, 90% N₂, <20ppm O₂) in modified Gifu Anaerobic Medium (mGAM; Nissui
384 Pharmaceuticals) broth buffered to pH 6.2 with 100mM 2-(N-morpholino)ethanesulfonic acid (MES;
385 Sigma-Aldrich). The redox indicator dye Resazurin (100µg/L media; Sigma-Aldrich) was added as a
386 quality control check for the presence of oxygen (turns red when conditions are not sufficiently
387 anaerobic). To prepare glycerol stocks, individual strains were first streaked onto mGAM agar (Nissui
388 Pharmaceuticals) and grown under anaerobic conditions (if possible, as not all strains can grow as single
389 colonies on agar-based media). The identity of each strain was confirmed using 16S rRNA sequencing
390 (Sanger sequencing; Source Biosciences) using the primers oOPC-953 and oOPC-954 for most species,
391 or g-Bifid-F and g-Bifid-R for Bifidobacteria (Table S3). Single colonies were then inoculated in
392 mGAM broth and stored at -70 degrees Celsius in mGAM with a final concentration of 25% glycerol.

393 **Genetic engineering of bacterial strains** Luminescence and fluorescence plasmids were transformed
394 into *K. pneumoniae* and *S. Typhimurium* using electroporation. Briefly, 5mL overnight culture was
395 washed 3x with cold Milli-Q water, before being concentrated in 500µl cold Milli-Q water. 2µl of
396 plasmid was mixed with 100µl of concentrated cells and electroporated (1.8kV; 0.1cm gap cuvettes)
397 before recovery in 1ml pre-warmed LB (1h at 37°C, shaking at 220rpm) and plating on LB with the
398 appropriate antibiotics.

399 Gene deletions were generated as described in (60). Briefly, 700 base pairs upstream and downstream
400 of region to be deleted were PCR amplified (Phusion[®], NEB) and inserted into the suicide vector pFOK,

401 which was linearised using the restriction enzymes BamHI and EcoRI, using the NEBuilder[®] HiFi DNA
402 Assembly (NEB). The plasmid was introduced into a diaminopimelic acid auxotroph *E. coli* strain
403 (JKe201). After 6h of mating between the plasmid-containing donor *E. coli* strain and the recipient *E.*
404 *coli*, *S. Typhimurium* or *K. pneumoniae* strain, trans-conjugants were selected on LB plates containing
405 50µg/mL kanamycin. Counter-selection was performed on no-salt LB plates supplemented with
406 0.5µg/mL of anhydrous tetracycline and 20% of sucrose at 30°C. Mutants were screened by colony
407 PCR and the sequence was verified using Sanger sequencing (Eurofins). Primers used for genetic
408 engineering in this study are listed in **Table S3**.

409 **Luminescence screen** *K. pneumoniae* (DSM 30104) and *S. Typhimurium* (SL1344) carrying a low
410 copy number plasmid with P_{nptII} promoter-driven expression of *luxCDBAE-frp* (pRSJ- $p_{nptII}::ilux$; also
411 known as the improved lux operon plasmid (*6I*)) were used for the luminescence screen. Symbiont
412 strains were tested in pairwise co-culture with the pathogens. All strains tested were first grown in
413 monoculture anaerobically in static mGAM broth buffered to pH 6.2 with 100mM MES at 37°C. *K.*
414 *pneumoniae* WT and *S. Typhimurium* WT carrying the luminescence plasmid pRSJ- $p_{nptII}::ilux$ were
415 separately incubated in the same media overnight.

416 *Competition assay*: once all strains had reached stationary phase (12-72 hours of growth depending on
417 the species), 20µL of each symbiont strain was dispensed in technical triplicates in a 96-well plate
418 containing 160µL of mGAM broth. 20µL of *K. pneumoniae* pRSJ- $p_{nptII}::ilux$ overnight culture or *S.*
419 *Typhimurium* pRSJ- $p_{nptII}::ilux$ overnight culture was then added to each well.

420 *Ecological invasion assay*: 180µL of each symbiont strain was dispensed in technical triplicates in a
421 96-well plate and 20µL *K. pneumoniae* pRSJ- $p_{nptII}::ilux$ overnight culture or *S. Typhimurium* pRSJ-
422 $p_{nptII}::ilux$ overnight culture was added to each well.

423 96-well plates from both assays were incubated anaerobically for 6 hours at 37°C. Before luminescence
424 measurement, 96-well plates were brought out of the anaerobic chamber and exposed to O₂ for 10
425 minutes because, critically, O₂ is needed for light production catalysed by the enzyme luciferase.
426 Luminescence at 515-575nm and OD-600nm were measured using a CLARIOstar Plus spectrometer
427 (BMG Labtech). Each data point (**Fig. S1**) represents the median of at least 3 independent biological
428 replicates (that is, using different overnight cultures of the same strain in different 96-well plates).

429 **Selection of the top and bottom ten symbiont strains from the screen** For each of the ecological
430 invasion and competition assays, symbiont strains were ordered from best- to worst-performing.
431 Symbiont strains were given two rankings: one from the competition assay and one from the invasion
432 assay. The two rankings were summed and ordered from lowest sum (best overall performing) to highest
433 sum (worst overall performing). From these ranks, the top ten and bottom ten strains were chosen. In

434 order to focus on the ability of non-pathogenic strains to limit colonization by pathogens, we decided
435 to focus for the community experiments on strains that have a category 1 safety level. Many common
436 gut bacteria cause occasional infections and therefore categorised as opportunistic pathogens with a
437 category 2 safety level, which can blur the line between being protective and causing disease. Removing
438 these strains took us from 100 to 54 strains. From these, we selected 50 species as our core set, removing
439 some strains that were duplicates of the same species.

440 **Construction of phylogenomic tree** The phylogenomic tree of strains in the luminescence screen
441 (n=100; **Fig. 1b-c; Table S1**) was inferred using default settings based on 67 single-copy core genes
442 using anvio v7.1 (62) and plotted using iTOL v6.7.5 (63).

443 **Extended competition assay** All culturing was performed in a shaking incubator at 225rpm and 37°C,
444 and under anaerobic conditions. Symbiont strains were grown to stationary phase (12-72 hours,
445 depending on the species), in Hungate tubes containing 5mL mGAM broth and 100mM MES and
446 buffered to pH 6.2. *K. pneumoniae* and *S. Typhimurium* carrying the fluorescence plasmid pBC11
447 (YPet) (64) were incubated overnight, with the appropriate antibiotics (**Table S1**).

448 Once in stationary phase, monocultures of symbionts were passaged (100µL culture into a new 5mL
449 tube of media) and grown for ~17 hours. Communities were assembled under anaerobic conditions into
450 new 5mL Hungate tubes (see section “community preparation”) and grown for 24 hours. Once grown,
451 communities were invaded with 100µl of the pathogen (10^6 cells/mL final concentration) in each
452 Hungate tube containing 5mL culture. Samples were taken immediately after addition of the pathogen
453 and prepared for measurement using flow cytometry (day 0). After 24 hours growth, the invaded
454 communities were sampled for flow cytometry (day 1) and 100µL was passaged into new tubes of 5mL
455 mGAM broth. After a further 24 hours, the end-point communities were sampled and measured a final
456 time (day 2).

457 For nutrient supplementation experiments (galactitol), 2.5mL mGAM buffered with 100mM MES to
458 pH 6.2 was prepared and autoclaved in Hungate tubes. A 2x stock solution of filter-sterilised sugar in
459 Milli-Q water (e.g. 0.2% or 2% galactitol) was prepared and de-oxygenated in the anaerobic chamber.
460 2.5mL of the stock solution was added into the Hungate tube to generate a 5ml total volume with the
461 appropriate concentration of the sugar. The extended competition experiment is performed as described
462 above, except samples were passaged again into tubes with the appropriate concentration of the sugar.
463 Samples were left to grow for 48h instead of the standard 24h to allow utilisation of low priority sugars,
464 such as galactitol.

465 For experiments with the AMR *E. coli* clinical isolate, the experiment was performed as described
466 above, except samples were analysed using selective plating instead of flow cytometry (LB + 100µg/mL
467 ampicillin to select for the AMR *E. coli* strain; MacConkey agar to enumerate total *E. coli* densities).

468 **Community preparation** All culturing was performed in a shaking incubator at 225rpm and 37°C, and
469 under anaerobic conditions. Constituent monocultures were grown to stationary phase, passaged into
470 new media and grown overnight for approximately ~17 hours, and then combined into communities.
471 The OD-600nm of the single strains was measured and the cultures were streaked anaerobically on
472 mGAM agar to check for contamination. Communities ranged from 2 to 50 strains in size and were
473 assembled under anaerobic conditions.

474 *In vitro*: For the communities containing 2-10 strains, equal volumes (100µL) of each overnight culture
475 were combined in a Hungate tube containing 5mL mGAM to form a community. For the 49- and 50-
476 strain communities, 20µL of each single strain was added, equating to a total volume of 1mL. The
477 communities were made by adding 1mL of each strain anaerobically to a 50mL falcon tube, mixing,
478 and removing 1mL to add to a fresh Hungate tube of 5mL mGAM broth. Communities were grown in
479 the shaking incubator (37°C, 225rpm) for 24 hours before being invaded with 10⁶ cells/mL of the
480 pathogen.

481 *In vivo*: Strains were grown separately, then OD-600nm of each culture was measured. For communities
482 containing 2-10 strains, the volume of culture containing 10⁹ cells was calculated for each individual
483 strain, based on a standard curve of OD-600nm and flow cytometry quantification. This was added to a
484 large falcon tube. The community mix was centrifuged (10 minutes, room temperature, 14000rpm) and
485 the resulting pellet resuspended in 2mL anaerobic PBS and kept on ice. 200µl were gavaged into each
486 mouse corresponding to 10⁸ cells for each strain. For the 49- or 50-strain communities, we used less
487 cells for each strain to avoid gavaging a large total cell density into mice (as done for the *in vitro*
488 experiments). The volume of culture containing 2*10⁸ cells was calculated for each constituent strain
489 and they were combined. The mixture was centrifuged and the pellet resuspended in 2mL PBS. Mice
490 were gavaged with 200µL of the inoculum. Therefore, the density of bacteria in the 200µL gavage was
491 equivalent for the 50-strain community as for the 10-strain community (10⁹ total cells). For all
492 inoculums, samples were taken for plating anaerobically on mGAM agar to confirm the cell density.

493 **Flow cytometry** Hungate tubes containing culture to be sampled were de-pressurised under anaerobic
494 conditions using needles. Samples were removed using needles and syringes. 10µL of each sample was
495 diluted in 90µL PBS + chloramphenicol 200µg/ml then 10µL added to a 96-well flat-bottomed plate
496 already containing 80µL PBS + chloramphenicol 200µg/ml. The 96-well plate was left to shake at room
497 temperature on the bench for 15 minutes to allow oxygen-dependent folding of YPet, while preventing
498 further growth of the sample with the bacteriostatic antibiotic chloramphenicol. Next, all bacterial cells

499 were fixed, permeabilised and fluorescently stained by adding 90µL PBS containing 4%
500 paraformaldehyde, 0.4% Triton X-100 and 1µg/mL 4',6-diamidino-2-phenylindole (DAPI) to each
501 sample well and incubating the plate in the dark for 1 hour at room temperature on a microplate shaker.
502 Prior to the measurement, 20µL AccuCheck counting beads (ThermoFisher- PBC100) was added to
503 every sample well. Two wells containing 200µL PBS were left between sample wells, in order to
504 prevent cross-contamination between samples. 96-well plates were run in a flow cytometer (Attune
505 NxT Autosampler with Attune NxT Flow Cytometer, ThermoFisher) set to: acquisition volume 50µL,
506 total draw volume 80µl, total sample volume 200µL, at a speed of 100µL/minute. Relevant spectral
507 parameters were recorded by the flow cytometer, equipped with 405nm, 488nm and 561nm lasers. The
508 following channels were used: DAPI staining, excitation 405nm, emission 415-465nm ('blue'); YPet
509 fluorescence, excitation 488nm, emission 505-515nm and 525-555nm ('green').

510 Flow cytometry data was processed using FlowJo v10.8.1 software. 'Beads' were gated on a linear
511 (FSC-H; SSC-H) axis. 'Bacteria' were gated on a logarithmic (FSC-H; SSC-H) axis. DAPI was gated
512 within the 'Bacteria' gate, on a logarithmic (Ex405-417; Ex405-495) axis. Within the DAPI gate, YPet
513 was gated on a logarithmic (Ex488-503; Ex488-555) axis. Count statistics for beads, DAPI and YPet
514 were exported to Microsoft Excel and pathogen density (cells/mL) was calculated.

515 **Mouse husbandry and experiments** Mouse experiments were performed with 6-8 weeks old germ-
516 free wild-type C57BL/6J female mice (RRID IMSR_JAX:000664) that were bred and maintained in
517 germ-free isolators at the Kennedy Institute, University of Oxford for more than five years. During
518 experiments, mice were housed as pairs or trios in sterile, individually ventilated Sentry SPP cages
519 (Allentown) with enrichment, irradiated food and autoclaved water. Cages of mice were disinfected in
520 TecCare Ultra Hydrogen peroxide, peracetic acid solution before mice were handled using individually
521 sterilised gloves (single use for each cage) in a biosafety cabinet that was disinfected with the same acid
522 solution in between each treatment group. Cages of mice were randomly assigned to a group, and cages
523 were opened in the same order each time. Researchers were not blinded because of the unbiased
524 quantification methods of colony counting and metagenomic sequencing. Samples sizes were
525 determined using standard practices of 7-8 mice per group distributed over 2-3 cages, and repeated the
526 experiment three times to allow experimental independence and sufficient power for nonparametric
527 testing. Mouse experiments were performed in accordance with the UK Animal Scientific Procedures
528 Act (1986) under a UK Home Office licence (PPL 9127884) assessed by the Medical Sciences Division
529 Animal Welfare and Ethical Review Body (AWERB) at the University of Oxford. Due to strictly
530 defined humane endpoints, one mouse needed to be terminated early. In this case, we excluded data
531 from that mouse.

532 Germ-free mice were gavaged with a 200µL inoculum of symbionts (see "community preparation") at
533 day -14 of the experiment and again on day -12 of the experiment (see scheme **Fig. 3a**). On day 0,

534 overnight cultures of the pathogens (*K. pneumoniae* and *S. Typhimurium*) grown aerobically in LB
535 containing the appropriate antibiotics were washed 3x with PBS and diluted. 10⁶ CFU of the pathogen
536 was given to each mouse as a 100µl gavage. Feces were sampled daily after gavage of the pathogen.
537 Fecal pellets were weighed and homogenised with a 5mm stainless steel bead in 1ml PBS (samples
538 were shaken vigorously in 2ml Eppendorf tubes). CFUs were enumerated using selective plating
539 (MacConkey or LB agar for *E. coli*; MacConkey + 50 µg/mL streptomycin for *S. Typhimurium*; LB +
540 50µg/mL carbenicillin for *K. pneumoniae*). *E. coli*, *K. pneumoniae* and *S. Typhimurium*, can be
541 differentiated by color on MacConkey agar (*S. Typhimurium* cannot utilise lactose) or morphology (*K.*
542 *pneumoniae* produces a capsule). Mice were euthanised 4 days after infection with the pathogen.

543 *S. Typhimurium* triggers inflammation to bloom in the gut (19). To allow us to focus on early
544 colonization events prior to triggering inflammation (i.e., colonization resistance), we used an avirulent
545 strain (SL1344 $\Delta invG \Delta ssaV$) to avoid triggering inflammation, disease and mortality (65).

546 **DNA isolation from feces and metagenomic sequencing** Aliquots of the feces were frozen
547 immediately after collection (prior to homogenisation in PBS) and stored at -80°C until use. Fecal
548 samples were thawed and resuspended in nuclease-free water, before being transferred to a lysing matrix
549 B tube (MP Biomedicals). 3 rounds of bead beating were performed at 6 m/s for 40s. Samples were
550 centrifuged at high speed and DNA in the supernatant was precipitated by adding sodium acetate (1/10
551 volume) and ice-cold ethanol (96-100%; equal volume), and left at -20°C overnight. Samples were
552 centrifuged at high speed and the pellet was washed twice with 70% ethanol, before being dried and
553 resuspended in nuclease-free water.

554 Samples were further purified using an AMPure clean-up protocol. The samples were mixed with
555 AMPure XP beads (Beckman Coulter) and incubated at room temperature for 5 minutes, before being
556 washed twice with 70% ethanol, using a magnet to avoid removing the DNA bound to the AMPure
557 beads. After air drying, nuclease-free water was added to the beads, to allow collection of the purified
558 DNA in the supernatant.

559 CosmosID performed metagenomic sequencing on isolated DNA. DNA libraries were prepared using
560 the Nextera XT DNA Library Preparation Kit (Illumina) and IDT Unique Dual Indexes. Prepared
561 libraries were sequenced on the Illumina NovaSeq 6000 platform 2x150bp (3M reads per sample).
562 CosmosID performed bioinformatic analysis according to proprietary methods on the raw data to
563 generate fine-grained taxonomic and relative abundance estimates (**Fig. S5**).

564 **Spent media assay** Strains were anaerobically inoculated, grown, passaged and assembled into
565 communities as described above. Communities were grown anaerobically in the shaking incubator
566 (225rpm, 37°C) for 96 hours to maximise depletion of nutrients utilisable by the community.
567 Supernatants were prepared by centrifuging the 96-hour cultures (10 minutes, 4400rpm, room

568 temperature) and filter-sterilising the supernatant (0.2µm filter). All preparation of supernatants were
569 done under anaerobic conditions. Two of each of the communities were assembled so that, for each
570 community, one Hungate tube containing 5mL supernatant and another Hungate tube containing 2.5mL
571 supernatant and 2.5mL mGAM (the re-supplemented treatment) were prepared. The supernatants were
572 invaded with 10^6 cells/mL of fluorescent pathogen, sampled and incubated for 24 hours as before.
573 Samples were taken on days 0 and 1.

574 **Nutrient utilisation overlap using biolog assays** Utilisation of carbon sources by symbionts and the
575 pathogens were assessed using AN Biolog Microplates™ (Biolog) according to the protocol of the
576 manufacturer. Briefly, strains were grown in mGAM and passaged (as detailed above). The cultures
577 were centrifuged anaerobically and washed twice in anaerobic PBS. The samples were concentrated
578 and an aliquot was taken to measure the OD-600nm. The cells were diluted or concentrated such that a
579 200µl aliquot of the cells would correspond to 65% transmittance (OD 0.187; the density outlined by
580 the manufacturer) in the 14ml volume of AN inoculating fluid provided. The concentrated cells were
581 added to the inoculating fluid aerobically (a small amount of O₂ is needed to oxidise the buffer) and
582 100µl was aliquoted into each well of the microplate. After 10min in aerobic conditions, the plates were
583 put in an air-tight container with a GasPak EZ Container System Sachet to generate hydrogen-free
584 anaerobic conditions. Samples were incubated at 35°C for 24h before measurement at 590nm. Since *S.*
585 *Typhimurium* SL1344 is a histidine auxotroph, a prototrophic strain was made using P22 transduction
586 (66) of the allele from a prototrophic strain of *S. Typhimurium* (ATCC 14028S). Positive clones were
587 selected for on M9 minimal media with 50µg/ml streptomycin and re-streaked 3 times on LB plates to
588 ensure phages are removed. Growth in the absence of exogenous histidine was validated by streaking
589 on M9 media.

590 For each plate, the absorbance reading at 590nm was subtracted from the blank (no carbon source
591 control in well A1). Each strain generates a different background signal so it is important to do this on
592 each plate individually. Each strain was measured as three independent biological replicates and the
593 median absorbance value was taken for each carbon source. We used a thresholding approach to
594 determine if a strain can metabolise a given carbon source (defined as Abs 590nm >0.1 median, after
595 blank subtraction; **Fig. S10**).

596 To predict overlap with the pathogens, whether a given strain can use a carbon source was compared to
597 the pathogen. We assessed which percentage of carbon sources that the pathogen can use can also be
598 used by the symbiont. To calculate overlap between pathogens and communities, we used an additive
599 calculation approach, where if a strain is contained in a community that can use a carbon source, the
600 entire community can use the carbon source. For simplicity, we did not treat cases where multiple
601 species use the same nutrients within the community differently than if a given nutrient is only covered
602 by one species.

603 **Genomic analysis using protein overlap** Genomic information from 50 symbiont strains and two
604 pathogens (*S. Typhimurium*, *K. pneumoniae*) were retrieved from the PATRIC database (67) (**Table**
605 **S1**). On this set, we applied a cluster-based analysis that groups proteins encoded in genomes into
606 PATRIC global protein families (68). A majority of symbiont strain proteins obtained a protein family
607 designation (clustering rate of 97.83%; 172 848 of 176 675) with protein families being populated by
608 proteins from on average 2.44 genomes (**Fig. S7**).

609 Based on this set, we drew protein family designations for focal symbiont communities and calculated
610 pathogen/community overlap using the same approach as for the Biolog plates above. That is, for each
611 protein family encoded in the pathogen's genome, we checked if it overlapped with any protein families
612 encoded in the community.

613 **Whole-genome sequencing** An overnight culture of *E. coli* 19Y000018 (the AMR clinical urine
614 isolate) was prepared in LB containing 100µg/ml ampicillin. A 1mL pellet was taken and DNA was
615 extracted using the same ethanol precipitation and AMPure clean-up protocol detailed above in the
616 section "DNA isolation from feces". Source BioScience performed whole-genome Illumina sequencing
617 on a NovaSeq 6000 to generate 10M 150bp paired end reads. Genome assembly was performed with
618 Unicycler v0.4.8 using default settings and subjected to protein family annotation as described in
619 "Genomic analysis using protein overlap".

620 **Predictions based on biologs and protein families** *Biolog-based predictions:* The carbon source
621 utilisation profile of the AMR *E. coli* clinical isolate was assessed using AN Biolog Microplates™ as
622 detailed above. Next, all possible communities made of 1, 2, 3, and 5 species were identified from the
623 16 symbiont strains that were previously analysed for carbon source utilisation. For each community,
624 the carbon source utilisation overlap was calculated (as detailed above; **Fig. 5a**). At each diversity level,
625 communities were sorted by overlap to the AMR *E. coli* clinical isolate. Given that the symbiont *E. coli*
626 is needed for colonization resistance in our experiments, we only included communities where the
627 symbiont *E. coli* is present. At each diversity level, we chose the highest ranked community (defined
628 "predicted best") and lowest ranked community (defined "predicted worst"). If there were ties in rank,
629 one community was randomly chosen. These communities were experimentally assessed for
630 colonization resistance using the extended competition *in vitro* assay as detailed above.

631 *Protein family-based predictions:* We used the whole-genome sequence of the AMR *E. coli* isolate to
632 calculate protein family overlap to communities of symbionts drawn from our 50-species community.
633 As for the biolog-based predictions, we restricted the analysis to communities that contained the
634 symbiont *E. coli* strain. Specifically, we generated 100,000 different communities randomly, each
635 containing the symbiont *E. coli* and a total of 2, 3, 5, or 10 species from the 50 species pool. We ranked
636 the communities according to their pathogen overlap at each diversity level and selected the highest and

637 lowest ranked communities for experimental validation. If ties occurred, we chose the communities at
638 random, as for the biolog-based predictions.

639 **Statistical analysis** All graphs were made and statistical analysis carried out in Prism v9.4.1
640 (GraphPad). Protein family overlap analyses and protein family-based predictions were computed in R
641 version v4.0.5 (69). Figure legends indicate the statistical test used and the sample sizes. Nonparametric
642 tests were used to avoid the assumptions of normality.

643 **Ethical statement** Mouse experiments were performed in accordance with the UK Animal Scientific
644 Procedures Act (1986) under a UK Home Office licence (PPL 9127884) assessed by the Medical
645 Sciences Division Animal Welfare and Ethical Review Body (AWERB) at the University of Oxford.
646 Mice were euthanised using cervical dislocation followed by exsanguination as a confirmation of death.

647

648 **References**

- 649 1. M. T. Sorbara, E. G. Pamer, Interbacterial mechanisms of colonization resistance and the
650 strategies pathogens use to overcome them. *Mucosal Immunol* **12**, 1-9 (2019).
- 651 2. A. Jacobson *et al.*, A Gut Commensal-Produced Metabolite Mediates Colonization Resistance
652 to Salmonella Infection. *Cell Host Microbe* **24**, 296-307 e297 (2018).
- 653 3. E. M. Velazquez *et al.*, Endogenous Enterobacteriaceae underlie variation in susceptibility to
654 Salmonella infection. *Nat Microbiol* **4**, 1057-1064 (2019).
- 655 4. S. Y. Wotzka *et al.*, Escherichia coli limits Salmonella Typhimurium infections after diet shifts
656 and fat-mediated microbiota perturbation in mice. *Nat Microbiol* **4**, 2164–2174 (2019).
- 657 5. R. P. Sequeira, J. A. K. McDonald, J. R. Marchesi, T. B. Clarke, Commensal Bacteroidetes protect
658 against Klebsiella pneumoniae colonization and transmission through IL-36 signalling. *Nat*
659 *Microbiol* **5**, 304-313 (2020).
- 660 6. C. G. Buffie *et al.*, Precision microbiome reconstitution restores bile acid mediated resistance
661 to Clostridium difficile. *Nature* **517**, 205-208 (2015).
- 662 7. S. G. Kim *et al.*, Microbiota-derived lantibiotic restores resistance against vancomycin-
663 resistant Enterococcus. *Nature* **572**, 665-669 (2019).
- 664 8. M. X. Byndloss *et al.*, Microbiota-activated PPAR-gamma signaling inhibits dysbiotic
665 Enterobacteriaceae expansion. *Science* **357**, 570-575 (2017).
- 666 9. R. A. Oliveira *et al.*, Klebsiella michiganensis transmission enhances resistance to
667 Enterobacteriaceae gut invasion by nutrition competition. *Nat Microbiol* **5**, 630-641 (2020).
- 668 10. G. Caballero-Flores, J. M. Pickard, G. Nunez, Microbiota-mediated colonization resistance:
669 mechanisms and regulation. *Nat Rev Microbiol* **21**, 347–360 (2023).
- 670 11. E. T. Granato, T. A. Meiller-Legrand, K. R. Foster, The Evolution and Ecology of Bacterial
671 Warfare. *Curr Biol* **29**, R521-R537 (2019).
- 672 12. C. Eberl *et al.*, E. coli enhance colonization resistance against Salmonella Typhimurium by
673 competing for galactitol, a context-dependent limiting carbon source. *Cell Host Microbe* **29**,
674 1680-1692 e1687 (2021).
- 675 13. L. Osbelt *et al.*, Klebsiella oxytoca causes colonization resistance against multidrug-resistant
676 K. pneumoniae in the gut via cooperative carbohydrate competition. *Cell Host Microbe* **29**,
677 1663-1679 e1667 (2021).

- 678 14. S. Caballero *et al.*, Cooperating Commensals Restore Colonization Resistance to Vancomycin-
679 Resistant *Enterococcus faecium*. *Cell Host Microbe* **21**, 592-602 e594 (2017).
- 680 15. S. Brugiroux *et al.*, Genome-guided design of a defined mouse microbiota that confers
681 colonization resistance against *Salmonella enterica* serovar Typhimurium. *Nat Microbiol* **2**,
682 16215 (2016).
- 683 16. A. G. Cheng *et al.*, Design, construction, and in vivo augmentation of a complex gut
684 microbiome. *Cell* **185**, 3617-3636 e3619 (2022).
- 685 17. S. Widder *et al.*, Challenges in microbial ecology: building predictive understanding of
686 community function and dynamics. *ISME J* **10**, 2557-2568 (2016).
- 687 18. E. Tacconelli *et al.*, Discovery, research, and development of new antibiotics: the WHO priority
688 list of antibiotic-resistant bacteria and tuberculosis. *Lancet Infect Dis* **18**, 318-327 (2018).
- 689 19. B. Stecher *et al.*, *Salmonella enterica* serovar typhimurium exploits inflammation to compete
690 with the intestinal microbiota. *PLoS Biol* **5**, 2177-2189 (2007).
- 691 20. S. E. Majowicz *et al.*, The global burden of nontyphoidal *Salmonella* gastroenteritis. *Clin Infect*
692 *Dis* **50**, 882-889 (2010).
- 693 21. C. L. Gorrie *et al.*, Gastrointestinal Carriage Is a Major Reservoir of *Klebsiella pneumoniae*
694 Infection in Intensive Care Patients. *Clin Infect Dis* **65**, 208-215 (2017).
- 695 22. M. M. Mayfield, D. B. Stouffer, Higher-order interactions capture unexplained complexity in
696 diverse communities. *Nat Ecol Evol* **1**, 62 (2017).
- 697 23. Y. Litvak, A. J. Baumler, The founder hypothesis: A basis for microbiota resistance, diversity in
698 taxa carriage, and colonization resistance against pathogens. *PLoS Pathog* **15**, e1007563
699 (2019).
- 700 24. K. Z. Coyte, S. Rakoff-Nahoum, Understanding Competition and Cooperation within the
701 Mammalian Gut Microbiome. *Curr Biol* **29**, R538-R544 (2019).
- 702 25. O. Manor *et al.*, Health and disease markers correlate with gut microbiome composition
703 across thousands of people. *Nat Commun* **11**, 5206 (2020).
- 704 26. C. A. Lozupone, J. I. Stombaugh, J. I. Gordon, J. K. Jansson, R. Knight, Diversity, stability and
705 resilience of the human gut microbiota. *Nature* **489**, 220-230 (2012).
- 706 27. C. Tropini *et al.*, Transient Osmotic Perturbation Causes Long-Term Alteration to the Gut
707 Microbiota. *Cell* **173**, 1742-1754 e1717 (2018).
- 708 28. K. V. Johnson, P. W. Burnet, Microbiome: Should we diversify from diversity? *Gut Microbes* **7**,
709 455-458 (2016).
- 710 29. A. Baichman-Kass, T. Song, J. Friedman, Competitive interactions between culturable bacteria
711 are highly non-additive. *Elife* **12**, e83398 (2023).
- 712 30. T. J. C. Ian Billick, Higher Order Interactions in Ecological Communities: What Are They and
713 How Can They be Detected? *Ecology* **75**, 15 (1994).
- 714 31. A. L. Gould *et al.*, Microbiome interactions shape host fitness. *Proc Natl Acad Sci U S A* **115**,
715 E11951-E11960 (2018).
- 716 32. W. B. Ludington, Higher-order microbiome interactions and how to find them. *Trends*
717 *Microbiol* **30**, 618-621 (2022).
- 718 33. S. Y. Wotzka *et al.*, Microbiota stability in healthy individuals after single-dose lactulose
719 challenge-A randomized controlled study. *PLoS One* **13**, e0206214 (2018).
- 720 34. S. B. Formal, G. J. Dammin, E. H. Labrec, H. Schneider, Experimental *Shigella* infections:
721 characteristics of a fatal infection produced in guinea pigs. *J Bacteriol* **75**, 604-610 (1958).
- 722 35. F. R. Blattner *et al.*, The complete genome sequence of *Escherichia coli* K-12. *Science* **277**,
723 1453-1462 (1997).
- 724 36. M. Ackermann *et al.*, Self-destructive cooperation mediated by phenotypic noise. *Nature* **454**,
725 987-990 (2008).
- 726 37. E. Gul *et al.*, The microbiota conditions a gut milieu that selects for wild-type *Salmonella*
727 Typhimurium virulence. *PLoS Biol* **21**, e3002253 (2023).

- 728 38. R. J. Gibbons, S. S. Socransky, B. Kapsimalis, Establishment of Human Indigenous Bacteria in
729 Germ-Free Mice. *J Bacteriol* **88**, 1316-1323 (1964).
- 730 39. R. Freter, H. Brickner, M. Botney, D. Cleven, A. Aranki, Mechanisms that control bacterial
731 populations in continuous-flow culture models of mouse large intestinal flora. *Infect Immun*
732 **39**, 676-685 (1983).
- 733 40. A. Wagner, Competition for nutrients increases invasion resistance during assembly of
734 microbial communities. *Mol Ecol* **31**, 4188-4203 (2022).
- 735 41. C. Antimicrobial Resistance, Global burden of bacterial antimicrobial resistance in 2019: a
736 systematic analysis. *Lancet* **399**, 629-655 (2022).
- 737 42. M. R. McLaren, B. J. Callahan, Pathogen resistance may be the principal evolutionary
738 advantage provided by the microbiome. *Philos Trans R Soc Lond B Biol Sci* **375**, 20190592
739 (2020).
- 740 43. M. J. Blaser, The theory of disappearing microbiota and the epidemics of chronic diseases. *Nat*
741 *Rev Immunol* **17**, 461-463 (2017).
- 742 44. M. Fassarella *et al.*, Gut microbiome stability and resilience: elucidating the response to
743 perturbations in order to modulate gut health. *Gut* **70**, 595-605 (2021).
- 744 45. H. C. Wastyk *et al.*, Gut-microbiota-targeted diets modulate human immune status. *Cell* **184**,
745 4137-4153 e4114 (2021).
- 746 46. E. Le Chatelier *et al.*, Richness of human gut microbiome correlates with metabolic markers.
747 *Nature* **500**, 541-546 (2013).
- 748 47. S. E. Winter *et al.*, Gut inflammation provides a respiratory electron acceptor for Salmonella.
749 *Nature* **467**, 426-429 (2010).
- 750 48. K. M. Pruss, J. L. Sonnenburg, *C. difficile* exploits a host metabolite produced during toxin-
751 mediated disease. *Nature* **593**, 261-265 (2021).
- 752 49. L. Maier *et al.*, Microbiota-derived hydrogen fuels Salmonella typhimurium invasion of the gut
753 ecosystem. *Cell Host Microbe* **14**, 641-651 (2013).
- 754 50. M. L. Jenior, J. L. Leslie, V. B. Young, P. D. Schloss, Clostridium difficile Colonizes Alternative
755 Nutrient Niches during Infection across Distinct Murine Gut Microbiomes. *mSystems* **2**,
756 e00063-00017 (2017).
- 757 51. K. M. Ng *et al.*, Microbiota-liberated host sugars facilitate post-antibiotic expansion of enteric
758 pathogens. *Nature* **502**, 96-99 (2013).
- 759 52. A. W. Hudson, A. J. Barnes, A. S. Bray, D. A. Ornelles, M. A. Zafar, Klebsiella pneumoniae l-
760 Fucose Metabolism Promotes Gastrointestinal Colonization and Modulates Its Virulence
761 Determinants. *Infect Immun* **90**, e0020622 (2022).
- 762 53. A. G. Jimenez, M. Ellermann, W. Abbott, V. Sperandio, Diet-derived galacturonic acid regulates
763 virulence and intestinal colonization in enterohaemorrhagic Escherichia coli and Citrobacter
764 rodentium. *Nat Microbiol* **5**, 368-378 (2020).
- 765 54. F. C. Pereira *et al.*, Rational design of a microbial consortium of mucosal sugar utilizers reduces
766 Clostridiodes difficile colonization. *Nat Commun* **11**, 5104 (2020).
- 767 55. E. Gul *et al.*, Differences in carbon metabolic capacity fuel co-existence and plasmid transfer
768 between Salmonella strains in the mouse gut. *Cell Host Microbe* **31**, 1140-1153 e1143 (2023).
- 769 56. N. Raffelsberger *et al.*, Gastrointestinal carriage of Klebsiella pneumoniae in a general adult
770 population: a cross-sectional study of risk factors and bacterial genomic diversity. *Gut*
771 *Microbes* **13**, 1939599 (2021).
- 772 57. S. K. Hoiseth, B. A. Stocker, Aromatic-dependent Salmonella typhimurium are non-virulent
773 and effective as live vaccines. *Nature* **291**, 238-239 (1981).
- 774 58. L. Maier *et al.*, Extensive impact of non-antibiotic drugs on human gut bacteria. *Nature* **555**,
775 623-628 (2018).
- 776 59. M. Tramontano *et al.*, Nutritional preferences of human gut bacteria reveal their metabolic
777 idiosyncrasies. *Nat Microbiol* **3**, 514-522 (2018).

- 778 60. F. R. Cianfanelli, O. Cunrath, D. Bumann, Efficient dual-negative selection for bacterial genome
779 editing. *BMC Microbiol* **20**, 129 (2020).
- 780 61. R. Soldan *et al.*, From macro to micro: a combined bioluminescence-fluorescence approach to
781 monitor bacterial localization. *Environ Microbiol* **23**, 2070-2085 (2021).
- 782 62. A. M. Eren *et al.*, Community-led, integrated, reproducible multi-omics with anvi'o. *Nat*
783 *Microbiol* **6**, 3-6 (2021).
- 784 63. I. Letunic, P. Bork, Interactive Tree Of Life (iTOL) v5: an online tool for phylogenetic tree display
785 and annotation. *Nucleic Acids Res* **49**, W293-W296 (2021).
- 786 64. O. Cunrath, D. Bumann, Host resistance factor SLC11A1 restricts Salmonella growth through
787 magnesium deprivation. *Science* **366**, 995-999 (2019).
- 788 65. S. Hapfelmeier *et al.*, The Salmonella pathogenicity island (SPI)-2 and SPI-1 type III secretion
789 systems allow Salmonella serovar typhimurium to trigger colitis via MyD88-dependent and
790 MyD88-independent mechanisms. *J Immunol* **174**, 1675-1685 (2005).
- 791 66. N. L. Sternberg, R. Maurer, Bacteriophage-mediated generalized transduction in Escherichia
792 coli and Salmonella typhimurium. *Methods Enzymol* **204**, 18-43 (1991).
- 793 67. A. R. Wattam *et al.*, Improvements to PATRIC, the all-bacterial Bioinformatics Database and
794 Analysis Resource Center. *Nucleic Acids Res* **45**, D535-d542 (2017).
- 795 68. J. J. Davis *et al.*, PATtyFams: Protein Families for the Microbial Genomes in the PATRIC
796 Database. *Front Microbiol* **7**, 118 (2016).
- 797 69. R Development Core Team, R. F. f. S. Computing, Ed. (Vienna, Austria, 2021).
- 798 70. F. Spragge and E. Bakkeren, M.T. Jahn, E.B.N. Araujo, C.F. Pearson, X. Wang, L. Pankhurst, O.
799 Cunrath, K.R. Foster. Data for: Microbiome diversity protects against pathogens by nutrient
800 blocking, Dryad (<https://doi.org/10.5061/dryad.pnvx0k6v8>) (2023).
- 801 71. F. Spragge and E. Bakkeren, M.T. Jahn, E.B.N. Araujo, C.F. Pearson, X. Wang, L. Pankhurst, O.
802 Cunrath, K.R. Foster. Code for: Microbiome diversity protects against pathogens by nutrient
803 blocking, GitHub (https://github.com/MartinTJahn/Nutrient_blocking) (2023).
- 804 72. B. Periaswamy *et al.*, Live attenuated S. Typhimurium vaccine with improved safety in
805 immuno-compromised mice. *PLoS One* **7**, e45433 (2012).
- 806 73. J. S. Johnson *et al.*, Evaluation of 16S rRNA gene sequencing for species and strain-level
807 microbiome analysis. *Nat Commun* **10**, 5029 (2019).
- 808 74. T. Matsuki *et al.*, Development of 16S rRNA-gene-targeted group-specific primers for the
809 detection and identification of predominant bacteria in human feces. *Appl Environ Microbiol*
810 **68**, 5445-5451 (2002).

811

812

813

814 **Acknowledgments**

815 We are indebted to members of the Foster lab for discussion, and to Emma Slack, Katharine Coyte,
816 Anna Weiss and Wolf-Dietrich Hardt for feedback on the manuscript. We thank Fiona Powrie and the
817 Oxford Centre for Microbiome Studies for germ-free mice and gnotobiotic mouse work. The
818 Heidelberg strains were a gift from Nassos Typas, EMBL Heidelberg. The AMR *E. coli* strain
819 19Y000018 was from Nottingham University Hospitals Pathogen Bank
820 (<https://www.nuh.nhs.uk/pathogen-industry/>). **Funding:** FS was supported by a BBSRC Studentship.
821 EB was supported by SNSF postdoc mobility fellowships (P2EZIP_199916 and P500PB_210941).
822 MTJ was supported by the Human Frontier Science Program (LT000798/2020). This work was
823 supported by Wellcome Trust Investigator award 209397/Z/17/Z and by European Research Council
824 Grant 787932 to KRF. **Author contributions:** Conceptualisation: KRF. Methodology: FS, EB, MTJ,
825 EBNA, CFP, XW, LP, OC. Investigation: FS, EB, MTJ, OC. Visualisation: FS, EB, MTJ. Funding
826 acquisition: KRF. Supervision: EB, OC, KRF. Writing – original draft: FS, EB, KRF. Writing –
827 review and editing: FS, EB, MTJ, CFP, XW, LP, OC and KRF. **Competing interests:** KRF holds
828 equity in Postbiotics Plus Research. **Data and materials availability:** All data used to generate the
829 plots is available via DRYAD (70). All code is available via GitHub (71). Metagenomic sequencing
830 and whole-genome sequencing of *E. coli* 0018 (NCBI accession number JAVXZX000000000) has
831 been deposited in SRA under the BioProject PRJNA1021490. There is no restriction on use of the
832 data, materials, or code, with the exception of *E. coli* strain 19Y000018 that is protected by an MTA
833 which requires permission from the Nottingham University Hospitals Pathogen Bank
834 (<https://www.nuh.nhs.uk/pathogen-industry/>). A Materials Design Analysis Reporting checklist is
835 supplied with the publication.

836 **License information:** Copyright © 2023 the authors, some rights reserved; exclusive licensee
837 American Association for the Advancement of Science. No claim to original US government works.
838 <https://www.science.org/about/science-licenses-journal-article-reuse>. This research was funded in
839 whole or in part by a Wellcome Trust Investigator award 209397/Z/17/Z, a cOAlition S organization.

840 The author will make the Author Accepted Manuscript (AAM) version available under a CC BY
841 public copyright license.

842

843 **Supplementary Materials**

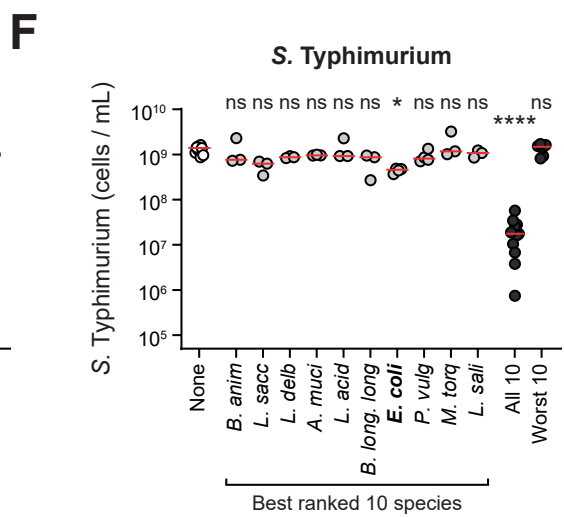
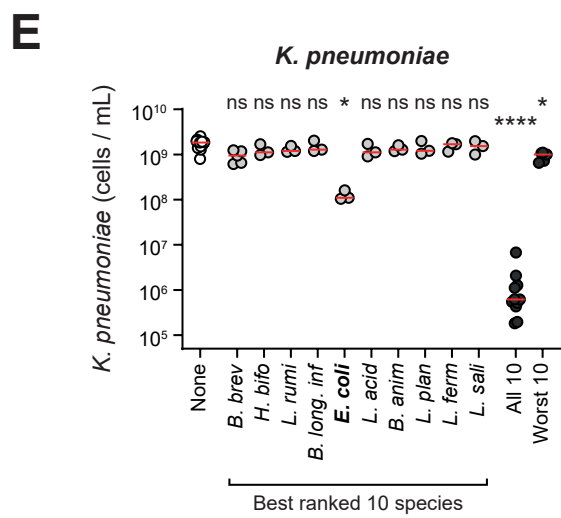
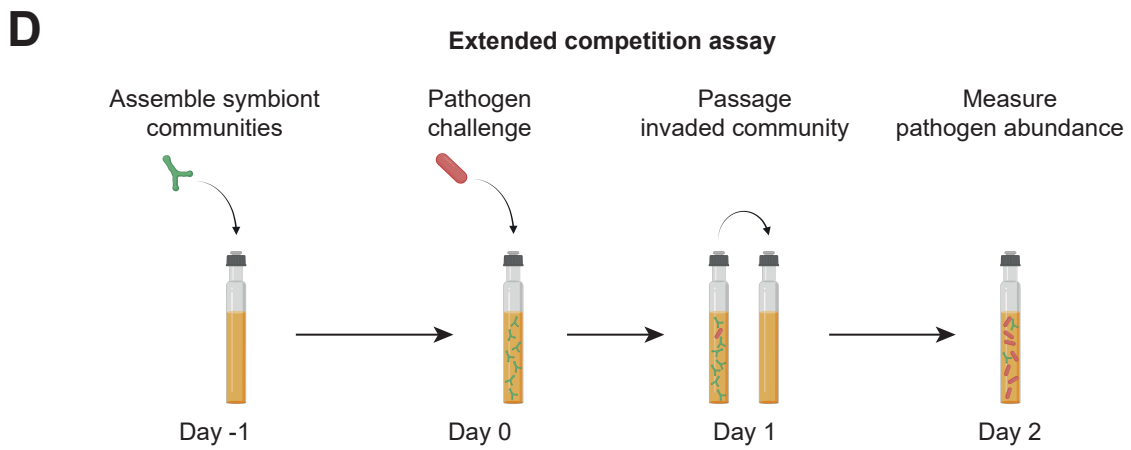
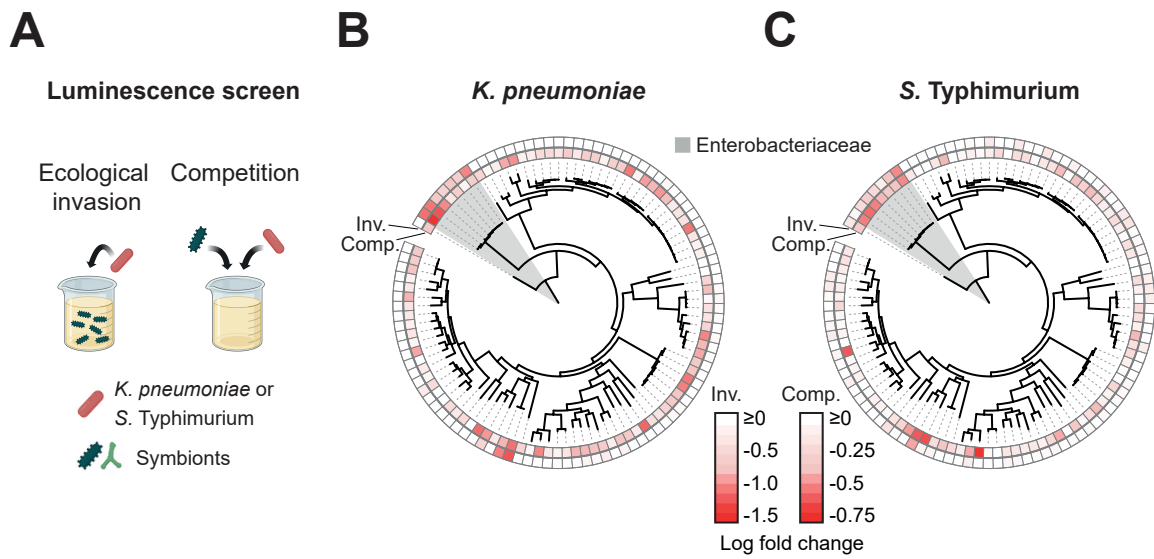
844 Figs. S1 to S13

845 Tables S1 to S7

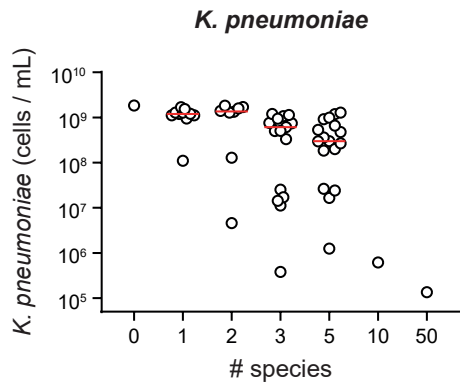
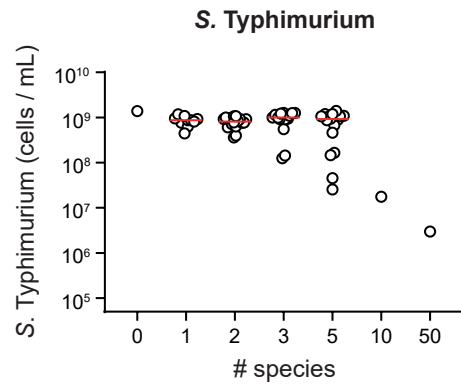
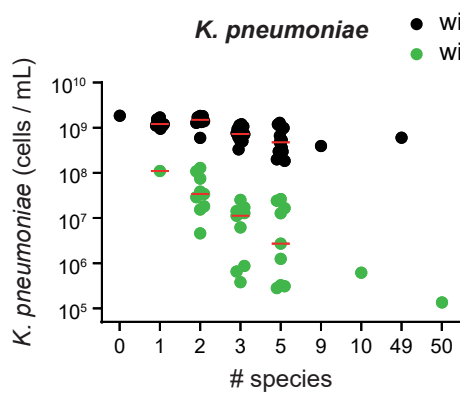
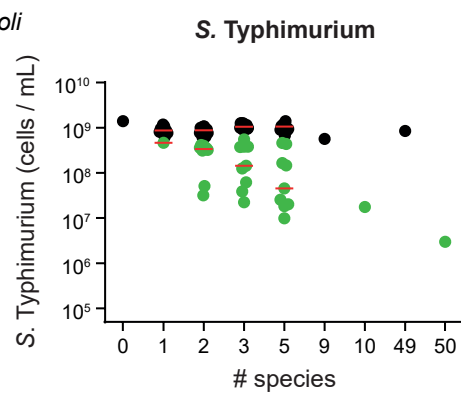
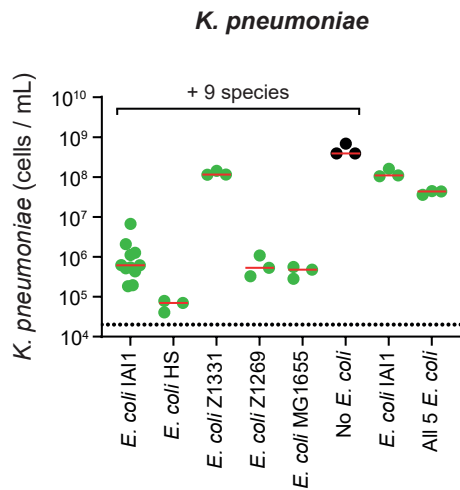
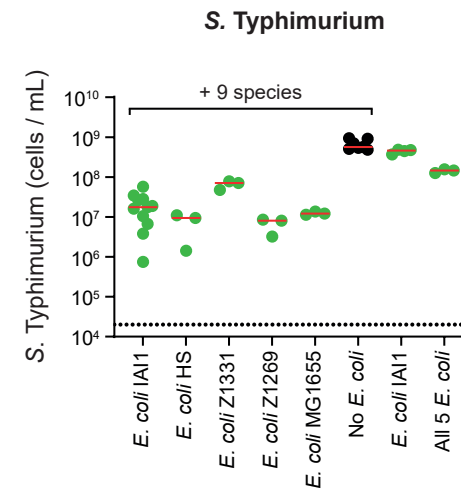
846 Supplementary references (72) – (74)

847

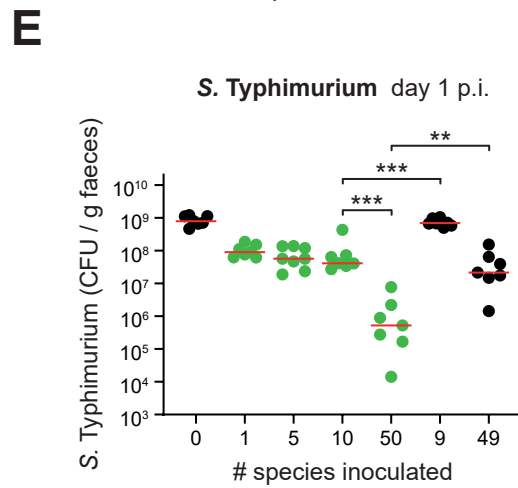
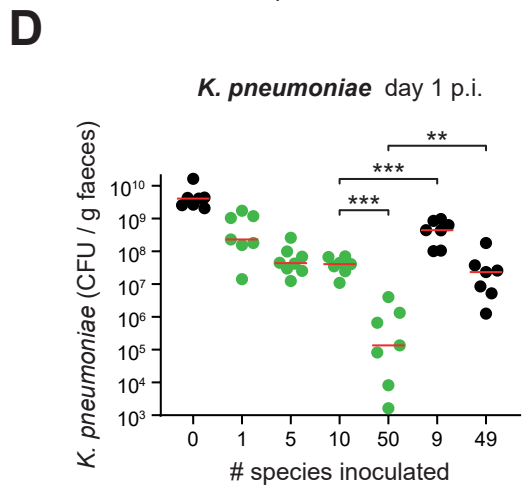
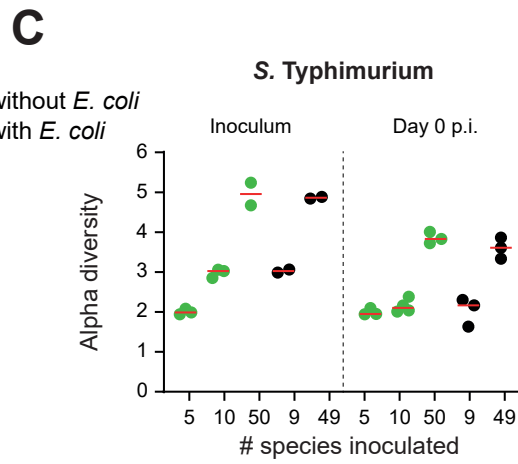
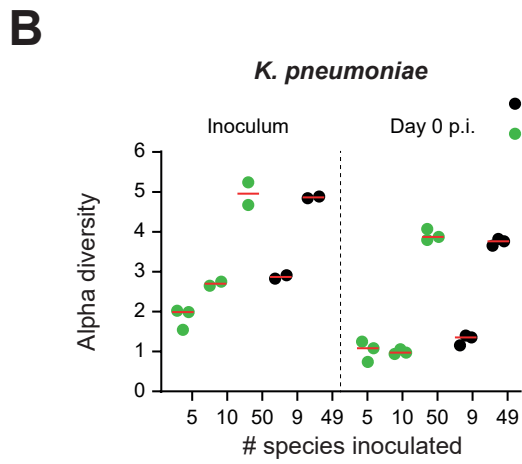
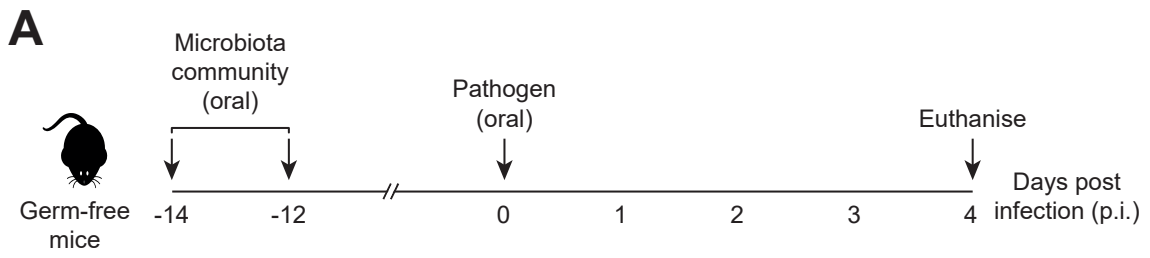
848 **Main figures and captions**



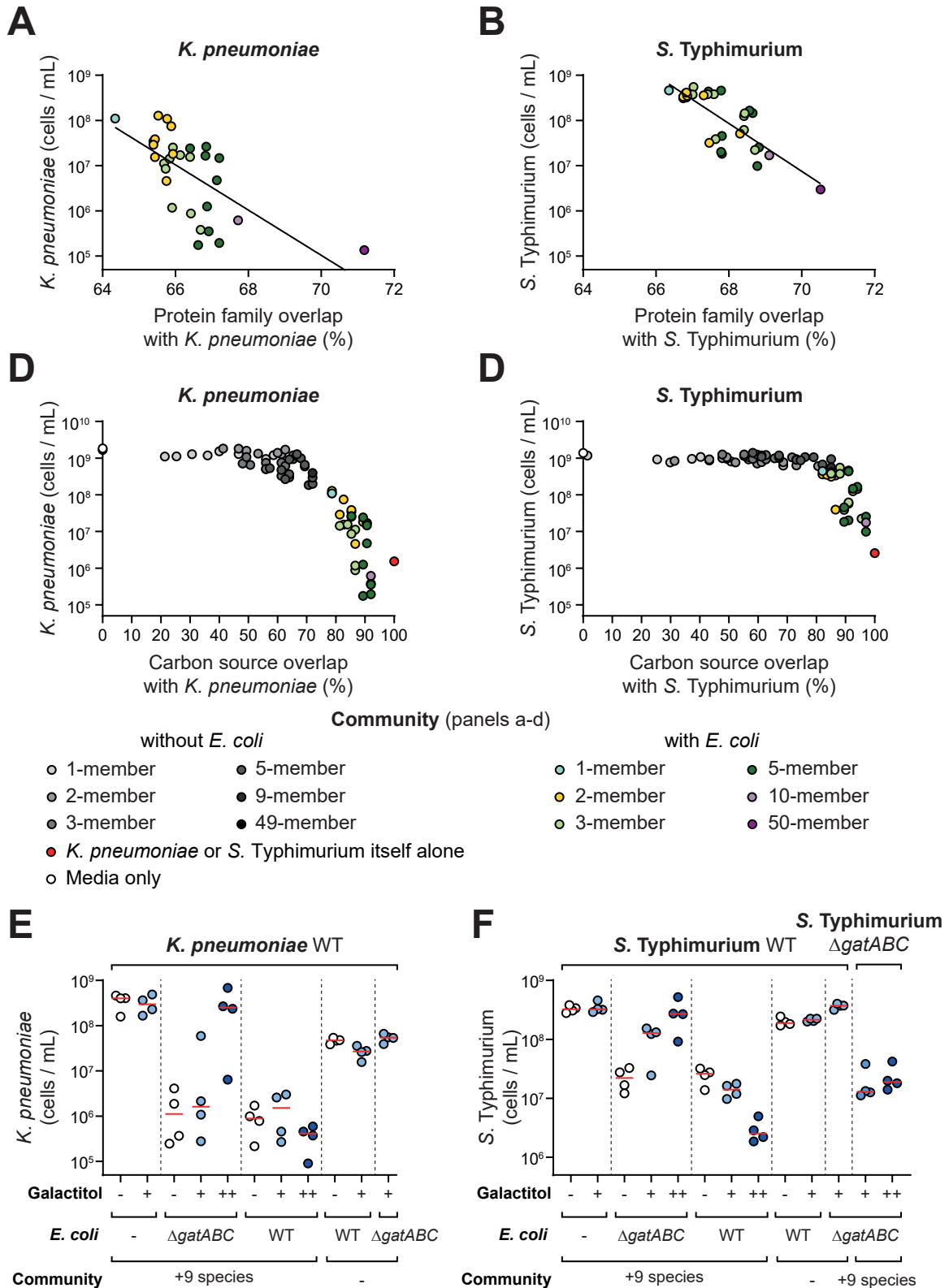
850 **Figure 1. Single strains do not provide robust colonization resistance, but a diverse community**
851 **can, depending on its composition. A)** Overview of the luminescence co-culture assays. In the
852 ecological invasion assay, *K. pneumoniae* or *S. Typhimurium* (red) was inoculated in co-culture with
853 individual symbionts (different green symbols are used to represent the diversity of symbiont species
854 screened; 19:1 ratio of symbiont to pathogen). In the competition assay, the symbionts were
855 inoculated at an equal ratio to the pathogen to recapitulate competition between strains once the
856 pathogen is established. In both assays, luminescence produced by the pathogen was used as a proxy
857 for pathogen growth. Created with BioRender.com. **B-C)** Comparison of phylogenetic relatedness
858 between symbionts, and the ability of each symbiont to compete with the pathogen (inv=ecological
859 invasion assay; comp=competition assay). Data for *K. pneumoniae* shown in **(B)** and *S. Typhimurium*
860 shown in **(C)**. The family Enterobacteriaceae, which includes both *K. pneumoniae* and *S.*
861 *Typhimurium*, is shaded in grey. Luminescence fold change values are presented in **Fig. S1**. Data
862 presented as the median luminescence log fold change of $N=3-10$ independent experiments
863 (biological replicates). Strains with the most negative (most red) values inhibited growth of the
864 pathogen most strongly. **D)** Overview of the extended competition assay. Communities (or individual
865 strains; green) of symbionts are pre-grown in anaerobic rich media before addition of the pathogen
866 (red). The community is passaged after 24h of growth, followed by another 24h of growth before
867 quantification with flow cytometry. Created with BioRender.com. **E-F)** The extended competition
868 assay was performed for each individual species identified in the best ranked 10 species, as well as for
869 combinations of 10 species (both the best- and worst-ranked 10 species; **Fig. S1**). Individual
870 biological replicates from $N=3-15$ independent experiments are shown. Red lines indicate the median.
871 A Kruskal-Wallis test with Dunn's multiple test correction compares each group to the no-symbionts
872 control ($p>0.05=ns$; $p<0.05=*$; $p<0.0001=****$). Data for *K. pneumoniae* shown in **(E)** and *S.*
873 *Typhimurium* shown in **(F)**. See **Table S1** for species name abbreviations.

A**B****C****D****E****F**

875 **Figure 2. Ecological diversity and key members are needed for efficient colonization resistance**
876 *in vitro*. **A-D)** Extended competition assay on communities made up of an increasing number of
877 species. Each data point represents the median pathogen cells/mL value on day 2 of the extended
878 competition for a community (n=3-15 biological replicates from independent experiments for each
879 community; up to 17 communities for each group). Communities with size ≤ 10 species were
880 randomly selected from the 10 best ranked species for each pathogen. Community identities are
881 shown in **Table S4-5**. Data for *K. pneumoniae* shown in **(A)** and **(C)**, and for *S. Typhimurium* shown
882 in **(B)** and **(D)**. Red lines indicate the median value of communities at a given diversity level. In **C-D)**,
883 data from **A-B)** are replotted along with additional communities that always contained *E. coli* but
884 were otherwise randomly selected. Communities without *E. coli* are depicted in black; communities
885 with *E. coli* in green. Separate red median lines shown for communities with and without *E. coli*. A
886 linear regression is performed on log-log transformed data in **Fig. S2a-b**, which shows that the
887 association between diversity and colonization observed is statistically significant, and that this effect
888 is greater for communities with *E. coli* than those without (F tests, $p \leq 0.0001$). **E-F)** Extended
889 competition assay testing *E. coli* strains substituted into the best ranked 10 species community. Data
890 for *K. pneumoniae* shown **(E)** and *S. Typhimurium* in **(F)**. Red lines indicate median values. Each
891 data point represents a biological replicate each from independent experiments ($N=3-11$).

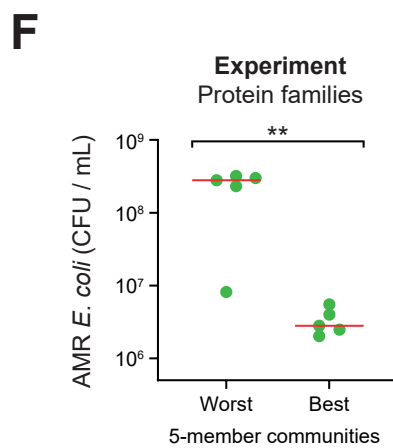
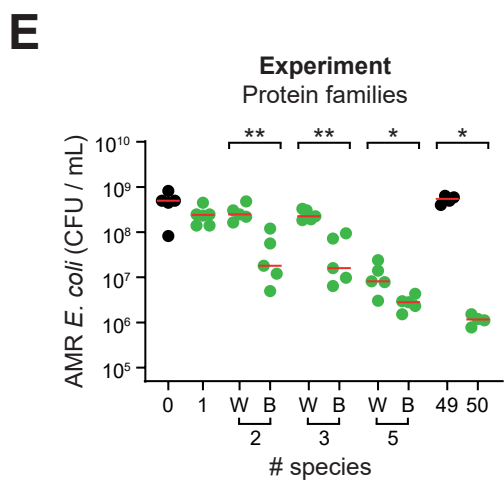
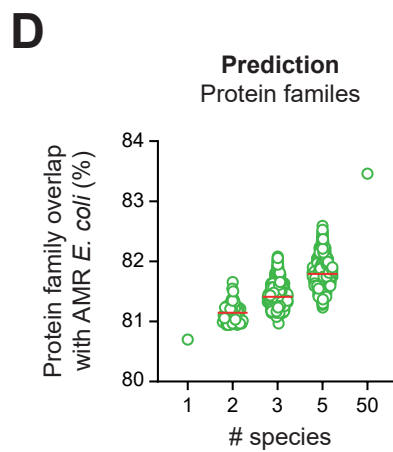
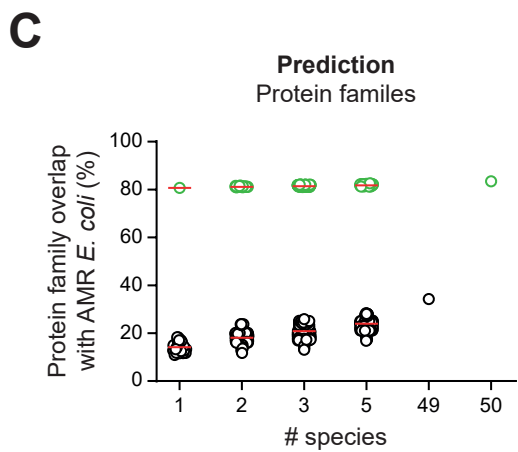
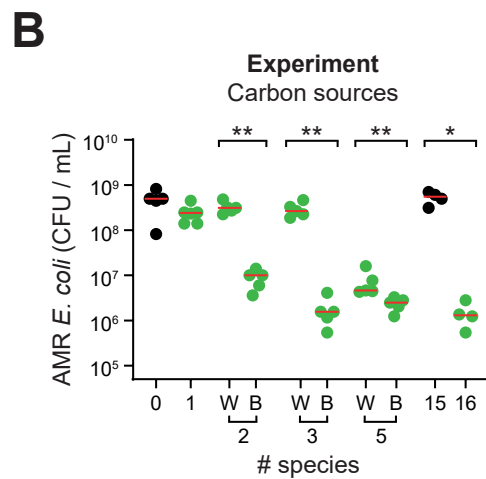
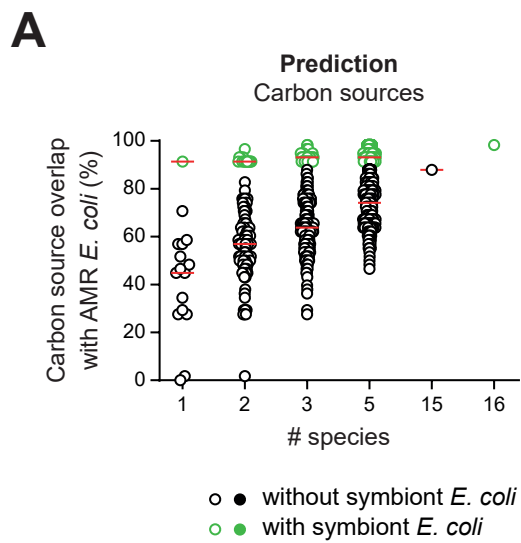


893 **Figure 3. Ecological diversity and key members are needed for efficient colonization resistance**
894 *in vivo*. **A)** Overview of gnotobiotic mouse experiments. Symbiont communities (or *E. coli* alone)
895 were given to germ-free mice by oral gavage twice (two days apart). 12 days later, the mice were
896 challenged with *K. pneumoniae* or *S. Typhimurium* by oral gavage. Feces were collected from mice
897 daily before being euthanised on day 4 post infection (p.i.). **B-C)** Alpha diversity measured by
898 Shannon index of symbiont communities. Metagenomic sequencing was performed on the inoculum
899 and fecal samples at day 0 (when the pathogen is introduced) and used to calculate diversity. Data for
900 *K. pneumoniae* shown in **(B)** and *S. Typhimurium* in **(C)**. Biological replicates from a representative
901 mouse from each cage are shown ($N=2-4$; at least two independent experiments). **D-E)** Pathogen
902 abundances in the feces of gnotobiotic mice colonized with communities of increasing diversity (mice
903 containing communities with *E. coli* shown in green; mice containing communities without *E. coli*
904 shown in black; $N=7-8$ biological replicates of mice per group in cages of 2-3 mice; 2-3 independent
905 experiments). Red lines indicate the medians. Two-tailed Mann-Whitney tests are used to compare the
906 indicated groups ($p<0.01=**$; $p<0.001=***$). Data for *K. pneumoniae* shown in **(D)** and *S.*
907 *Typhimurium* shown in **(E)**. Metagenomic analysis of strain diversity and relative abundance is
908 shown in **Fig. S5**. Pathogen abundance data from days 1-4 p.i. is shown in **Fig. S6**. Community
909 compositions are shown in **Table S6**.



911 **Figure 4. Nutrient overlap can explain the role of ecological diversity and the effect of *E. coli* in**
912 **colonization resistance. A-B)** Protein family overlap is compared to the median pathogen abundance
913 values for each community containing *E. coli* from **Fig. 2C-D**. Diversity is visualised by a color
914 gradient. Data for *K. pneumoniae* shown in **(A)** and *Salmonella* shown in **(B)**. A line of best fit is
915 shown from a linear regression on log transformed data: $R^2 = 0.4255$ for *K. pneumoniae*; $R^2 = 0.603$
916 for *S. Typhimurium*; both slopes are significantly different from 0 using an F-test ($p < 0.0001$). Data
917 for communities without *E. coli* is presented in **Fig. S9E-F**. **C-D**. Overlap in carbon source utilisation
918 plotted against the median pathogen abundance measurements from experimental communities in **Fig.**
919 **2C-D**. Community carbon source overlap is calculated using an additive approach from carbon source
920 overlap of individual strains by measurement on AN Biolog Microplates (**Fig. S10**). Diversity is
921 visualised by a gradient of color (for *E. coli*-containing communities) or greyscale (for communities
922 without *E. coli*). A control with the isogenic pathogen itself (100% overlap) is plotted in red. Data for
923 *K. pneumoniae* in **(C)** and *S. Typhimurium* shown in **(D)**. **E-F**) A private nutrient, galactitol, that
924 could only be used by the WT *E. coli* strain and the pathogens but not by the other symbionts nor an
925 *E. coli* $\Delta gatABC$ mutant, was supplemented to the media and the extended competition assay
926 performed as before. In all treatments, pathogen abundance was measured by flow cytometry after
927 48h of growth post-passage instead of the usual 24h. This change did not influence the control
928 experiments without galactitol, but proved informative because we found the growth impacts of
929 galactitol were relatively slow. Results for *K. pneumoniae* shown in **(E)** and *S. Typhimurium* in **(F)**.
930 $N=3-4$ biological replicates from independent experiments per treatment. Horizontal red lines show
931 the median of the replicates. Light blue circles show results with 0.1% galactitol supplementation (+
932 symbol), dark blue circles show results with 1% galactitol supplementation (++ symbol). White
933 circles (control) show results with no nutrient supplementation (- symbol). 9 species refers to the 9
934 additional species in the 10 best-performing species for each respective pathogen (- symbol refers to
935 when *E. coli* is added alone). In **(D)**, a $\Delta gatABC$ mutant of *S. Typhimurium* was used in addition to
936 the WT pathogen to verify the dependency of colonization on a private nutrient.

937



939 **Figure 5. Nutrient blocking predicts community colonization resistance. A)** *In silico* prediction of
940 carbon source overlap with the AMR *E. coli* strain for all possible combinations of symbiont
941 communities at the indicated diversity levels. Each circle represents a different community.
942 Communities containing the symbiont *E. coli* IAI1 are shown in green and communities without *E.*
943 *coli* IAI1 are shown in black (predictions as hollow circles; experimental data as solid circles).
944 Predicted carbon source overlap calculated using an additive approach from carbon source use of
945 individual strains measured using AN Biolog MicroPlates (**Fig. S10, S13**). **B)** Experimental test of *in*
946 *silico* predictions in **(A)**. The two *E. coli* IAI1-containing communities predicted to have the best **(B)**
947 and worst **(W)** carbon source overlap were picked at each diversity level and competed against AMR
948 *E. coli* in the extended competition assay. A two-tailed Mann-Whitney U test was performed on
949 community pairs ($p > 0.05 = \text{ns}$; $p < 0.05 = *$; $p < 0.01 = **$) at the 2-, 3- and 5-strain diversity levels. Red
950 horizontal bars depict the median of each community tested. $N = 4-5$ biological replicates from
951 independent experiments for each community. **C-D)** *In silico* prediction of protein family overlap
952 with the AMR *E. coli* strain for a random subset ($n = 59,043$) of all possible symbiont communities at
953 diversity levels 2-, 3-, and 5-strains, as well as all individual strains and the 49- and 50-species
954 communities. Each circle represents a different community. Communities are selected from the strains
955 comprising the 50-member community. Communities containing *E. coli* IAI1 are shown in green and
956 communities without *E. coli* IAI1 are shown in black. **D)** Only the *E. coli*-containing communities are
957 plotted to better visualise variation in protein family overlap. **E)** Experimental test of *in silico*
958 predictions based on protein cluster overlap in **(C-D)**. The two *E. coli* IAI1-containing communities
959 predicted to have the best **(B)** and worst **(W)** protein family overlap were picked at each diversity
960 level (randomly selected, for cases where there were multiple communities with the same overlap),
961 and competed against AMR *E. coli* in the extended competition assay. Red horizontal bars depict the
962 median of each community tested. $N = 5$ biological replicates from independent experiments for each
963 community. A two-tailed Mann-Whitney U test was performed on community pairs ($p > 0.05 = \text{ns}$;
964 $p < 0.05 = *$; $p < 0.01 = **$) at the 2-, 3- and 5-strain diversity levels. **F)** Experimental test of the predicted
965 5 best and 5 worst communities at the 5-strain diversity level, based on protein family overlap with

966 AMR *E. coli*. Each symbol represents the median of N=5 biological replicates from independent
967 experiments per community. Red horizontal bars depict the median of the best and the worst predicted
968 communities. A two-tailed Mann-Whitney U test was performed ($p < 0.01 = **$). Community identities
969 for **(B, E-F)** are shown in **Table S7**.

970
971
972
973
974
975
976
977
978
979
980
981
982
983
984
985
986
987
988
989
990
991
992



Supplementary Materials for

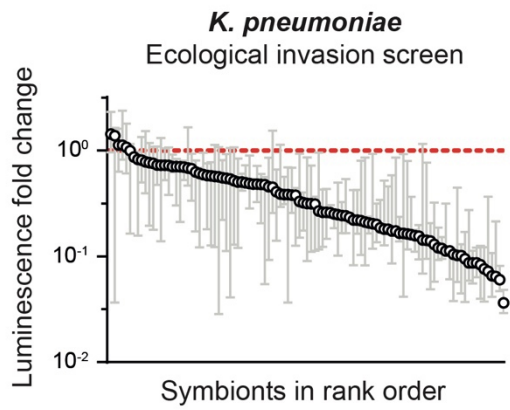
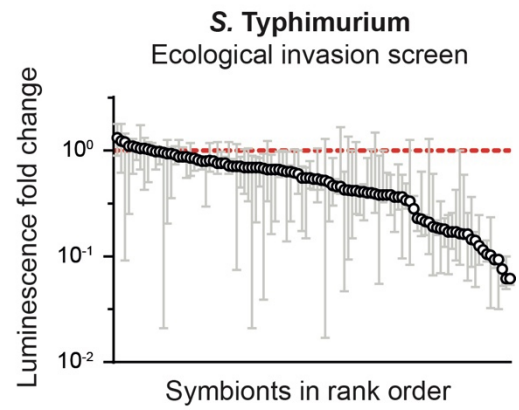
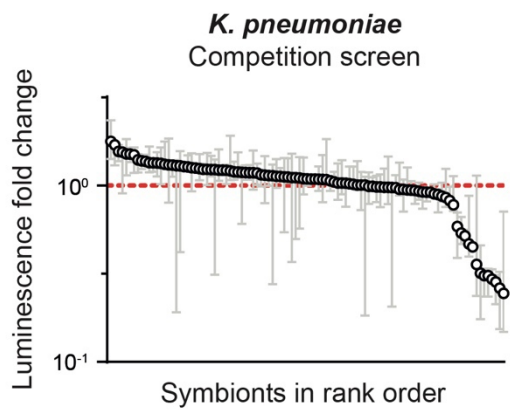
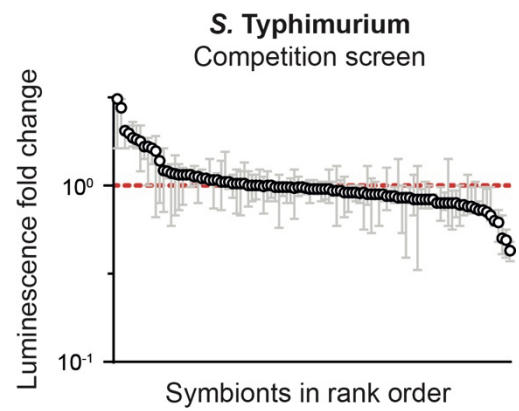
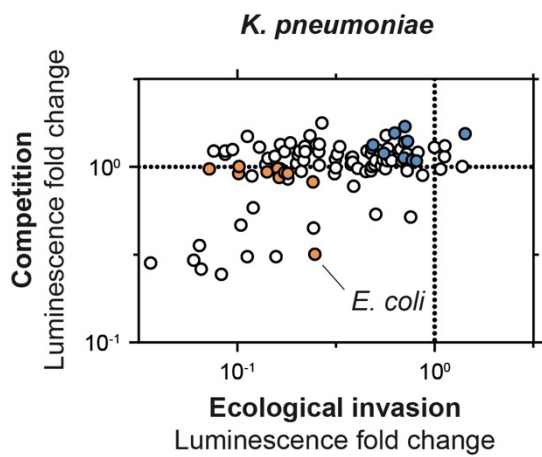
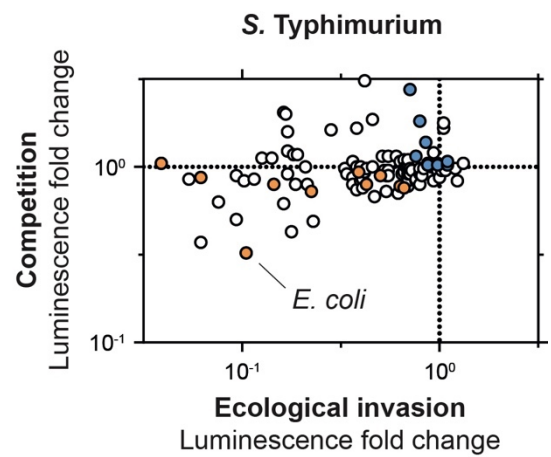
Microbiome diversity protects against pathogens by nutrient blocking

Frances Spragge⁺ and Erik Bakkeren⁺, Martin T. Jahn, Elizete B. N. Araujo, Claire F. Pearson, Xuedan Wang, Louise Pankhurst, Olivier Cunrath* and Kevin R. Foster*

*Correspondence to: kevin.foster@biology.ox.ac.uk; olivier.cunrath@unistra.fr; ⁺These authors contributed equally to this work.

This PDF file includes:

- Figs. S1 to S13
- Tables S1 to S7
- Supplementary references (72) – (74)

A**B****C****D****E****F**

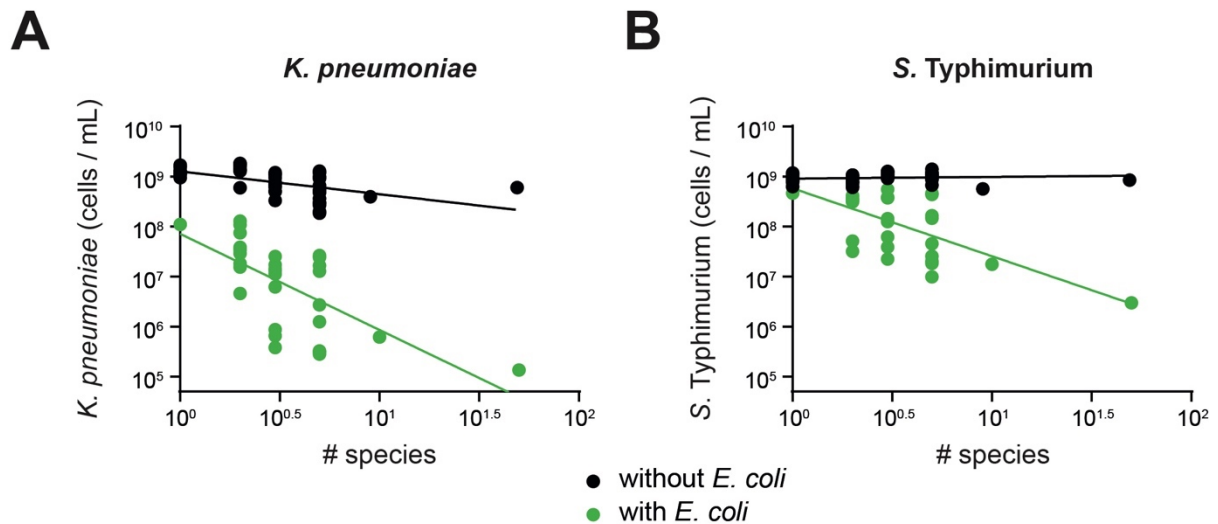
- Ten **best** ranked species
- Ten **worst** ranked species
- Other symbionts

993

994 **Fig. S1.**

42

995 **Human gut symbiont strains vary in their ability to inhibit growth of *K. pneumoniae* and**
996 ***S. Typhimurium* in the luminescence screen. A-D)** Waterfall plots show the luminescence
997 median fold change (log ratio of the control luminescence divided by the treatment
998 luminescence) of the pathogen in combination with each human gut symbiont tested in the
999 luminescence screen. Results for *K. pneumoniae* are shown in (A) and (C) and for *S.*
1000 *Typhimurium* shown in (B) and (D). Results of the ecological invasion assay are shown in (A)
1001 and (B) and the competition assay in (C) and (D). Black circles represent the median value for
1002 each symbiont ($N=3-10$ biological replicates from independent experiments). Grey vertical
1003 lines represent range bars. E-F) Correlation of the results of the ecological invasion and
1004 competition assays of the luminescence screen. Each circle represents the median value for a
1005 symbiont ($N=3-10$ biological replicates from independent experiments). Results for *K.*
1006 *pneumoniae* shown in (E) and *S. Typhimurium* in (F). The sum of the ranks of the competition
1007 and the ecological invasion assays were used to create an overall ranking of symbionts for each
1008 pathogen. The best 10 ranked species are shown in orange and the worst 10 shown in blue, with
1009 the added criteria that they have a category 1 safety level (see Methods). Strains with the most
1010 negative competition and invasion values inhibited the growth of the pathogen most strongly
1011 compared to the media-only control.
1012



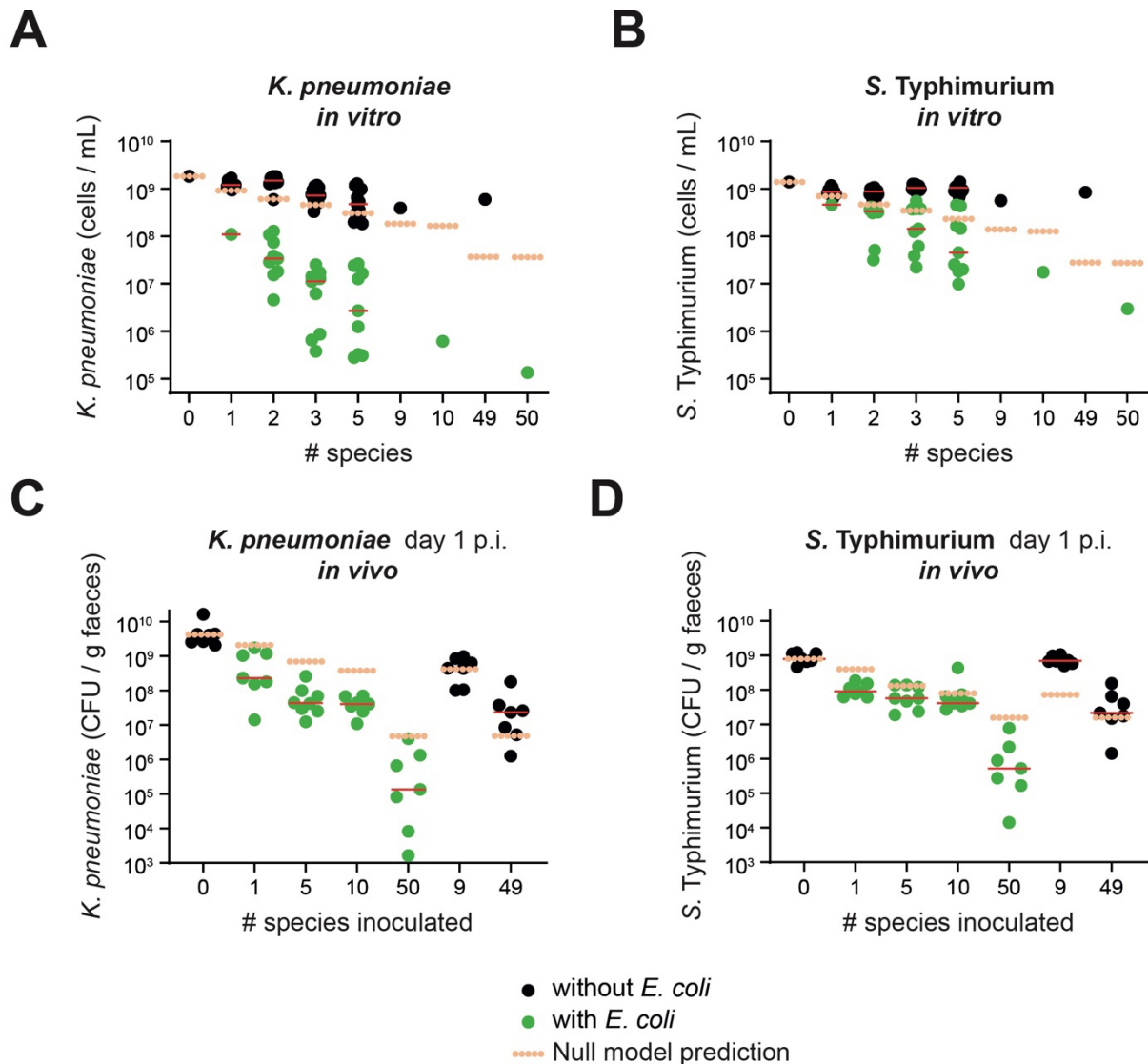
1013

1014 **Fig. S2.**

1015 **Community diversity negatively correlates with pathogen abundance. A-B)** As the number
 1016 of symbiont strains increases, pathogen density on day 2 of the extended competition decreases
 1017 (x axis on a log scale). Data for *K. pneumoniae* shown in **(A)** and *S. Typhimurium* in **(B)**. Each
 1018 circle represents the median value of a community tested in the extended competition assay
 1019 (data from **Fig. 2C-D**). Communities in green contain *E. coli*, communities in black do not
 1020 contain *E. coli*. Linear regression of log-transformed data: **(A)** $R^2=0.4296$, non-zero slope for
 1021 *E. coli* communities (F test, $p<0.0001$). $R^2=0.3103$, non-zero slope for communities without *E.*
 1022 *coli* (F test, $p<0.0001$). Moreover, slopes of the two regressions are significantly different from
 1023 each other (F test, $p=0.0001$). **(B)** $R^2=0.4234$, non-zero slope for *E. coli* communities (F test,
 1024 $p<0.0001$). $R^2=0.01378$, slope not different to zero for communities without *E. coli* (F test,
 1025 $p=0.4218$). Slopes of the two regressions are again significantly different from each other (F
 1026 test, $p<0.0001$).

1027

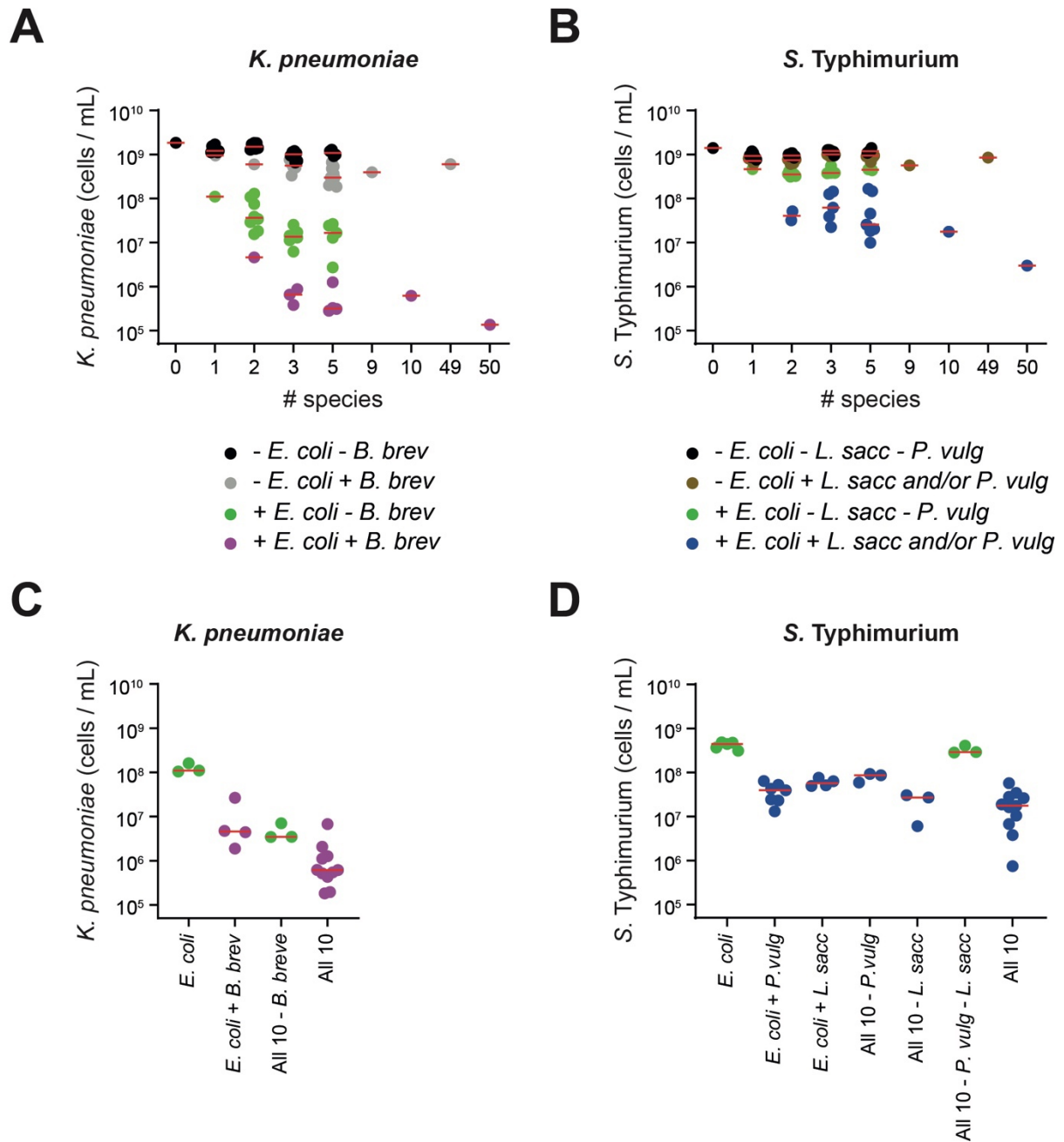
1028



1029

1030 **Fig. S3.**

1031 **Comparison to a null model where the effect of each species proportionally restricts**
 1032 **pathogen growth in an additive manner.** We compared our experimental data to a null model
 1033 where the effect of colonization resistance simply scales according to the number of species in
 1034 the community. Specifically, we took the abundance of the pathogen at the end of the
 1035 experiment when the pathogen is alone (ie, $n=0$) and multiplied it by $1/(n)$ where n refers to the
 1036 number of species that contribute to the overall carrying capacity of the system (including the
 1037 pathogen). This value is plotted in as beige dotted lines for both *in vitro* data from **Fig. 2C-D**
 1038 (panels A and B; dots indicate median values of each community) and *in vivo* data from **Fig.**
 1039 **3D-E** (panels C and D; dots indicate individual mice). **A,C)** Data for *K. pneumoniae*, **B,D)**
 1040 Data for *S. Typhimurium*. Communities containing *E. coli* are shown in green and communities
 1041 without *E. coli* are shown in black. Red lines indicate medians. In all cases, the deviation
 1042 between the null model and data increases at higher diversities, so long *E. coli* is present in the
 1043 high diversity communities. This effect is also statistically significant in all cases: we compare
 1044 the ratio of predicted to observed pathogen abundance for 1 species data to that from the 50
 1045 species case (Two-tailed Mann-Whitney U tests; $p=0.0070$ for **panel A**; $p=0.0070$ for **panel**
 1046 **B**; $p=0.0041$ for **panel C**; $p=0.0262$ for **panel D**).

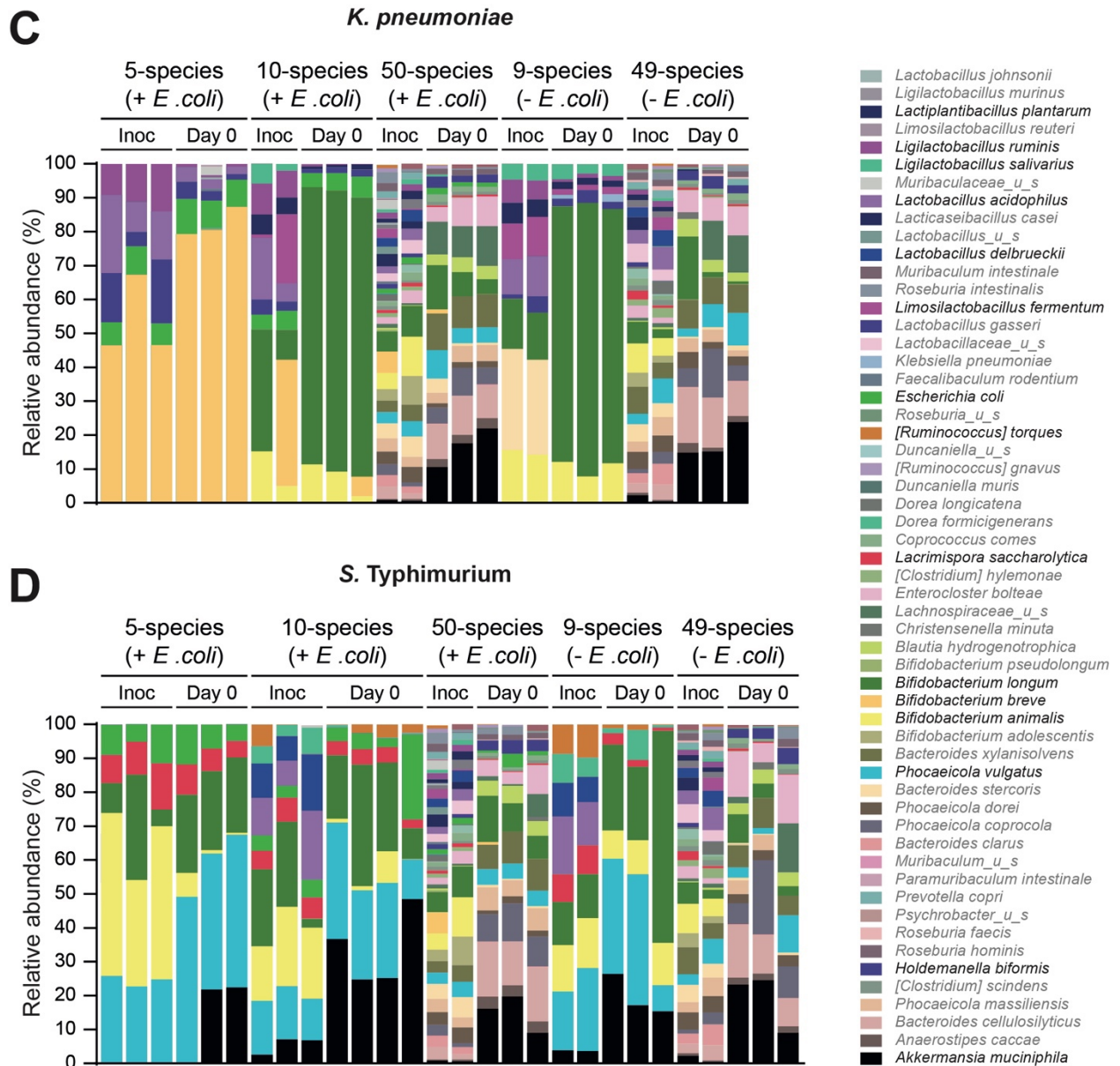
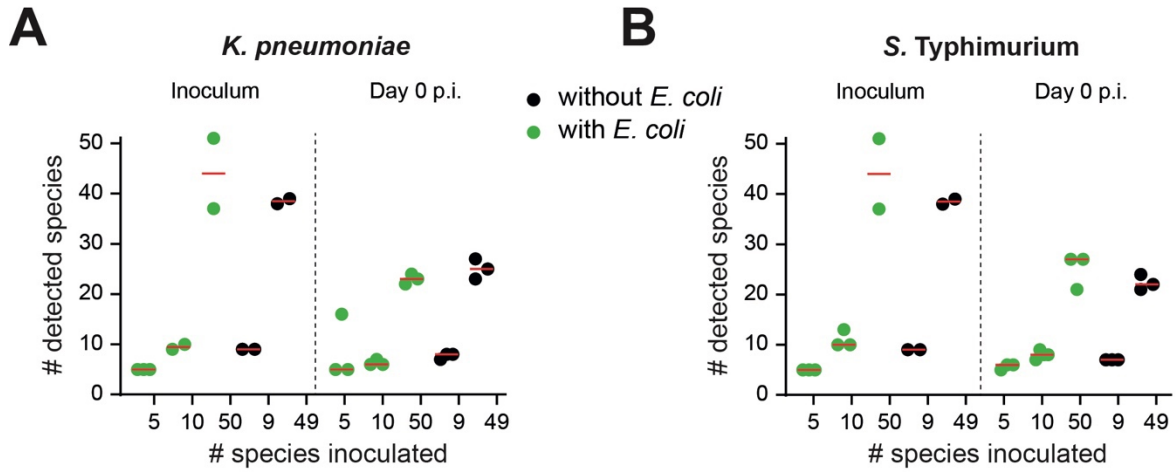


1048

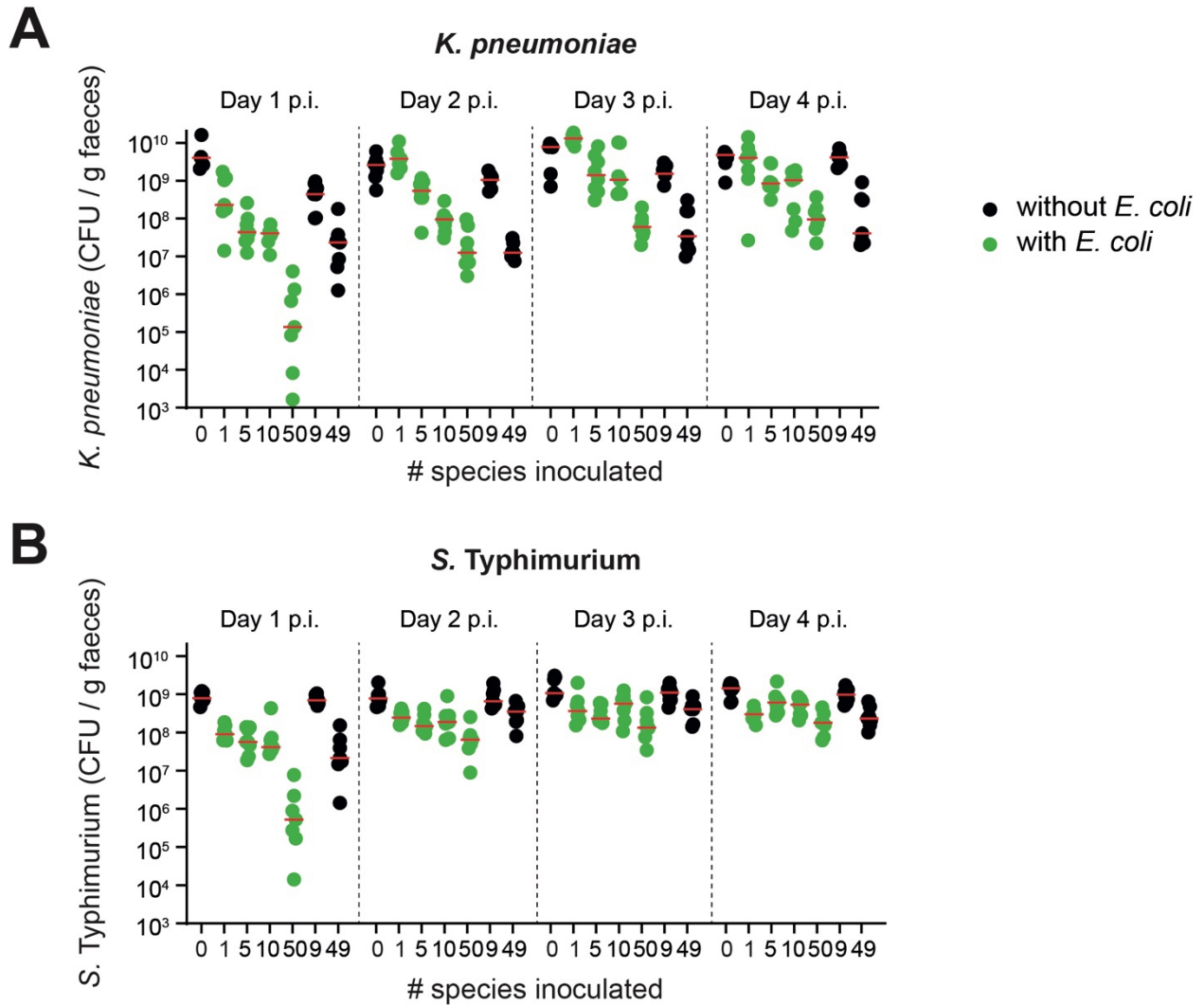
1049 **Fig. S4.**

1050 **Combinations of multiple species are important for colonization resistance to each**
 1051 **pathogen. A-B)** Equivalent figures to **Fig. 2C-D**, except the presence or absence of *B. breve*
 1052 within communities are shown in **(A)** (grey for communities with *B. breve* but without *E. coli*
 1053 and purple for communities with *B. breve* and *E. coli*), and the presence or absence of *L.*
 1054 *saccharolyticum* and/or *P. vulgatus* shown in **(B)** (brown for communities with *L.*
 1055 *saccharolyticum* and/or *P. vulgatus* but not *E. coli*, and blue for communities with *L.*
 1056 *saccharolyticum* and/or *P. vulgatus* and *E. coli*). Results for *K. pneumoniae* are shown in **(A)**
 1057 and for *S. Typhimurium* shown in **(B)**. In **(A-B)**, “+” and “-” refer to the presence or absence
 1058 of species rather than the addition or subtraction of a species. Horizontal red lines depict the
 1059 median of the communities at a particular diversity level containing the species indicated in the
 1060 legend. Each circle represents the median pathogen abundance measured for a community on
 1061 day 2 of the extended competition assay. **C-D)** Drop-out experiments verify the context-

1062 dependent effect of key members on colonization resistance. $N=3-11$ biological replicates from
1063 independent experiments. In **(C-D)**, “+” and “-” refer to the addition or subtraction of a species.
1064 Results for *K. pneumoniae* are shown in **(C)** and for *S. Typhimurium* shown in **(D)**. Horizontal
1065 red lines depict the median of the replicates for a particular community. See **Table S1** for
1066 species name abbreviations.
1067



1069 **Fig. S5.**
1070 **Metagenomic sequencing shows that germ-free mice gavaged with more diverse**
1071 **communities were colonized with a higher number of bacterial strains. A-B)** Number of
1072 detected bacterial species (above a relative abundance threshold of 0.1%) in the inoculum given
1073 to the mice and in mouse feces 14 days after the first inoculum gavage (Day 0 post infection;
1074 p.i.). Mice were given 2 identical gavages containing symbiont communities 2 days apart; the
1075 first inoculum was sequenced as a representative. Each inoculum data point depicts an
1076 independent experiment and each day 0 data point indicates a representative mouse from each
1077 cage. Horizontal red lines represent median values of the replicates at each diversity level.
1078 ($N=2-3$ for the inoculum, $N=3-4$ for fecal samples; data indicates biological replicates of a
1079 representative mouse from each cage, derived from at least two independent experiments).
1080 Green symbols represent communities that contain *E. coli*, black symbols represent
1081 communities without *E. coli*. **C-D)** Relative abundance plot of symbiont strains in the inoculum
1082 and mouse feces using metagenomic sequencing data. Data for mice challenged with *K.*
1083 *pneumoniae* shown in **(C)** and *S. Typhimurium* in **(D)**. The 10 best ranked strains from the
1084 luminescence screen for each pathogen are shown in black writing (other detected species in
1085 grey writing).

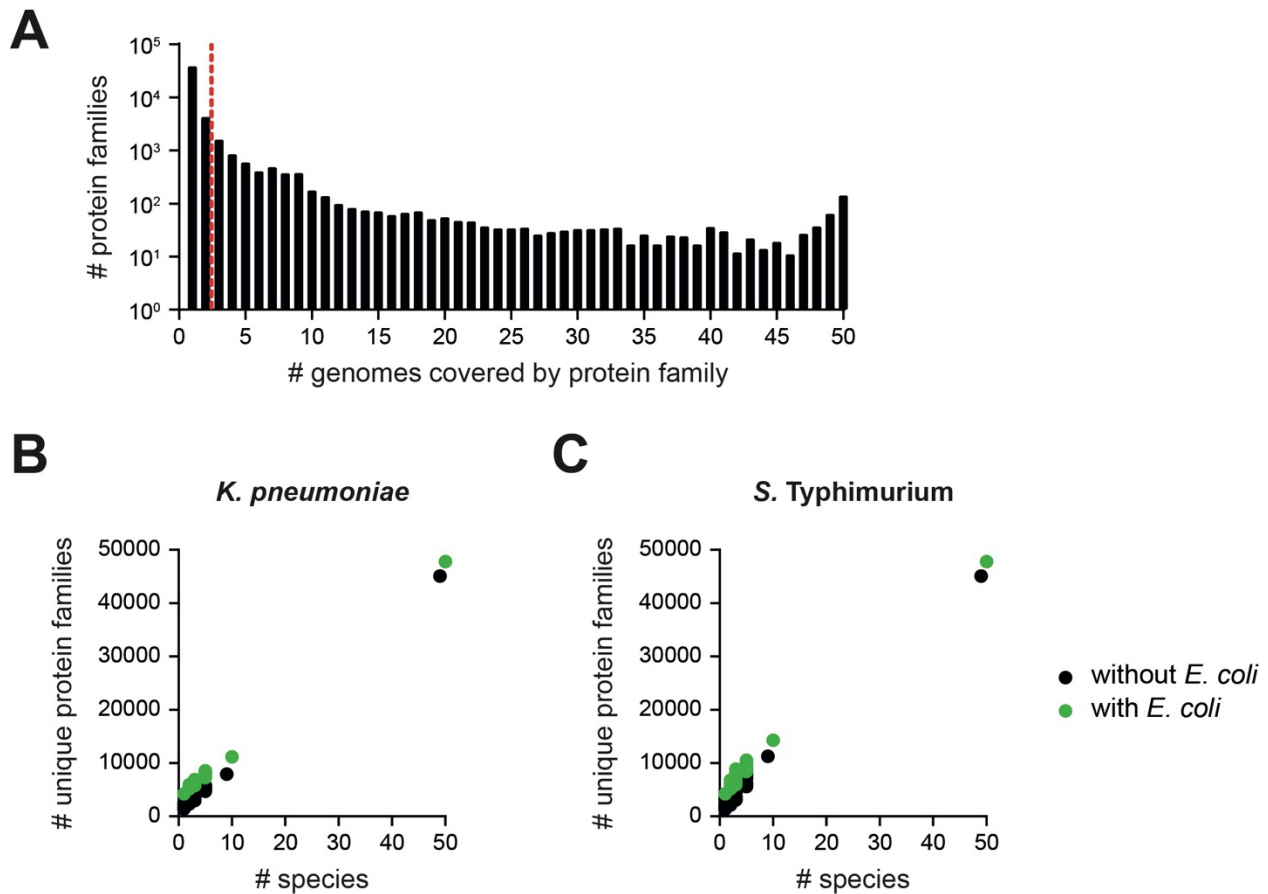


1086

1087 **Fig. S6.**

1088 **Pathogen abundance *in vivo* at later timepoints. A-B)** Mice were gavaged with *K.*
 1089 *pneumoniae* (A) or *S. Typhimurium* (B) on Day 0. Each symbol represents a fecal sample from
 1090 1 mouse. Pathogen abundances were determined by selective plating aerobically on LB agar +
 1091 carbenicillin (*K. pneumoniae*) or LB agar + streptomycin (*S. Typhimurium*). Horizontal red
 1092 lines represent median values of the replicate mice tested at each diversity level. Communities
 1093 containing *E. coli* are shown in green whereas communities without *E. coli* are in black. $N=7-$
 1094 8 biological replicates of mice per group in cages of 2-3 mice; 2-3 independent experiments.
 1095 The day 1 post infection (p.i.) data is the same as in **Fig. 3D-E**.

1096



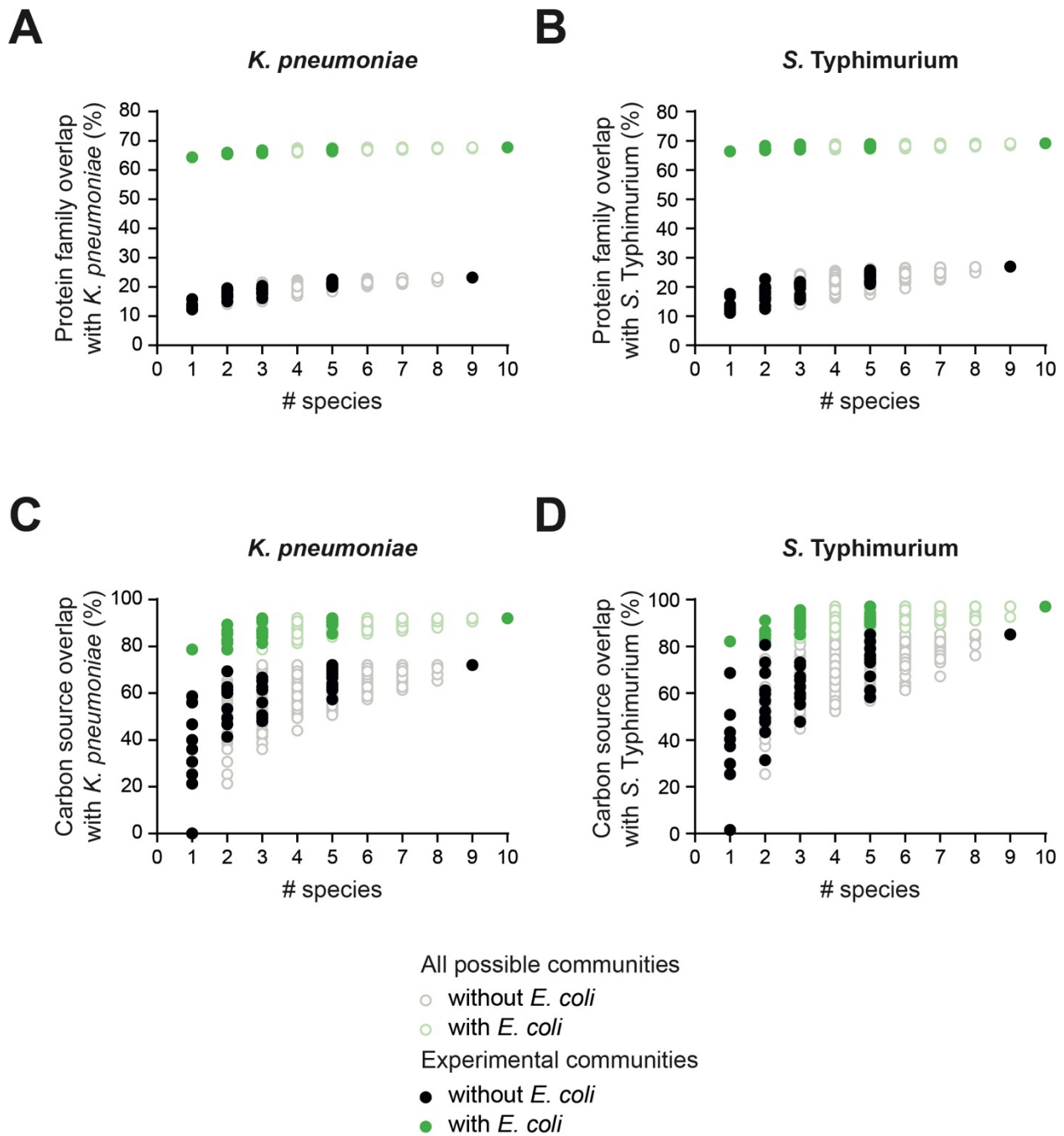
1097

1098 **Fig. S7.**

1099 **The number of protein families increase proportional to community diversity. A)**

1100 Histogram showing the distribution of protein families among the 50 species subset used for
 1101 protein family analysis. The vertical red dashed line represents the average number of genomes
 1102 out of the 50 strains that share a particular protein family (2.44 genomes). There is an average
 1103 of 3.22 proteins in each protein family. The histogram shows that many protein families are
 1104 unique to a strain while others (141) are shared between all 50 strains. **B-C)** The number of
 1105 protein families covered by a community increases as the number of strains in the community
 1106 increases. Results for *K. pneumoniae* shown in **(B)** and for *S. Typhimurium* in **(C)**. Community
 1107 IDs taken from **Fig. 2C-D**. Each circle represents a different community. Green circles depict
 1108 communities containing *E. coli*, while black circles are communities without *E. coli*.

1109



1110

1111 **Fig. S8.**

1112 **The randomly chosen communities used in the *in vitro* experiments are representative of**

1113 **all possible combinations of the 10 best-ranked species. A-B) Experimental communities**

1114 **contain representative protein family overlap to the pathogens compared to all possible**

1115 **combinations of the 10 best-ranked species. All possible combinations of communities are**

1116 **depicted by unfilled circles, experimentally tested communities are shown as filled circles.**

1117 **Communities in green contain *E. coli* while communities in black do not contain *E. coli*. Data**

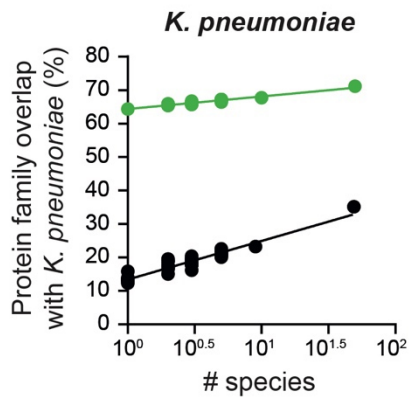
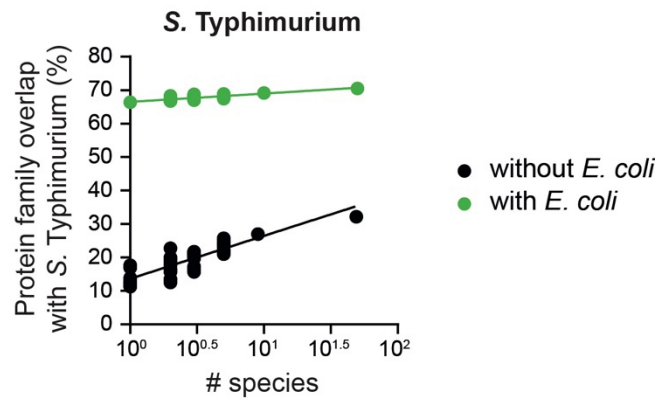
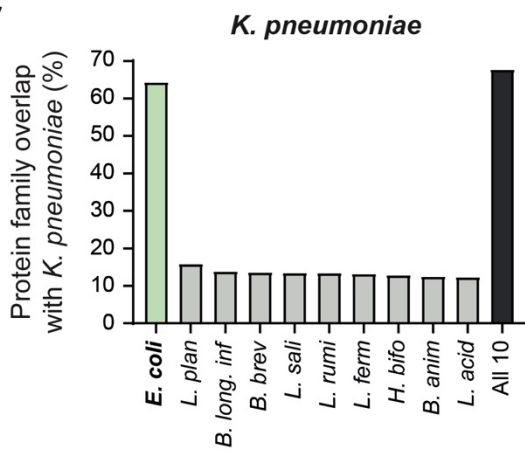
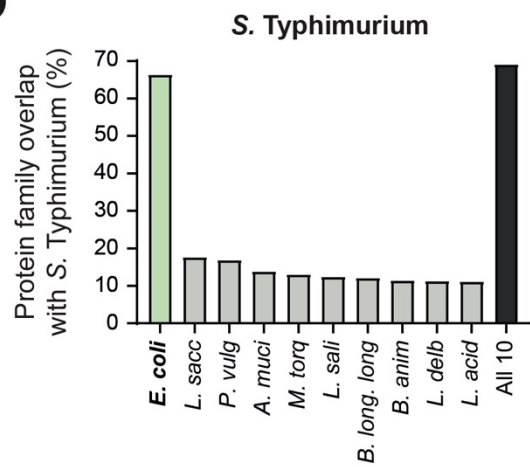
1118 **for *K. pneumoniae* shown in (A) and for *S. Typhimurium* in (B); data from Fig. 2C-D. C-D)**

1119 **Experimental communities contain representative carbon source utilization overlap to the**

1120 **pathogens compared to all possible combinations of the 10 best-ranked species. All possible**

1121 **combinations of communities are depicted by unfilled circles, experimentally tested**

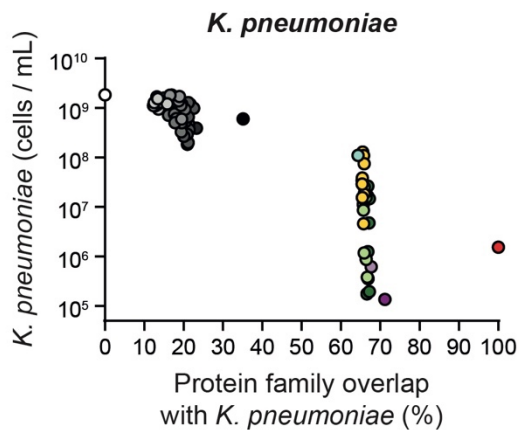
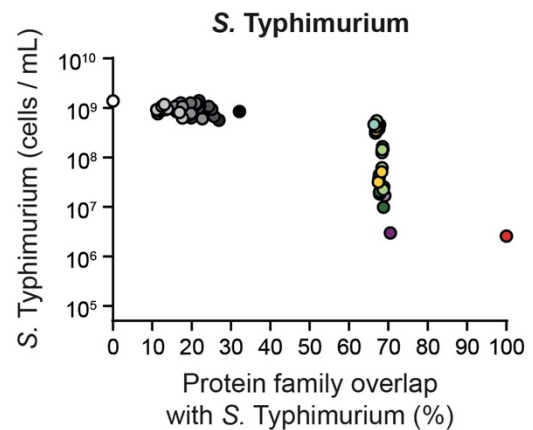
1122 communities are shown as filled circles. Communities in green contain *E. coli* while
1123 communities in black do not contain *E. coli*. Data for *K. pneumoniae* shown in **(C)** and for *S.*
1124 Typhimurium in **(D)**.
1125

A**B****C****D****Community composition (panels e-f)**without *E. coli*

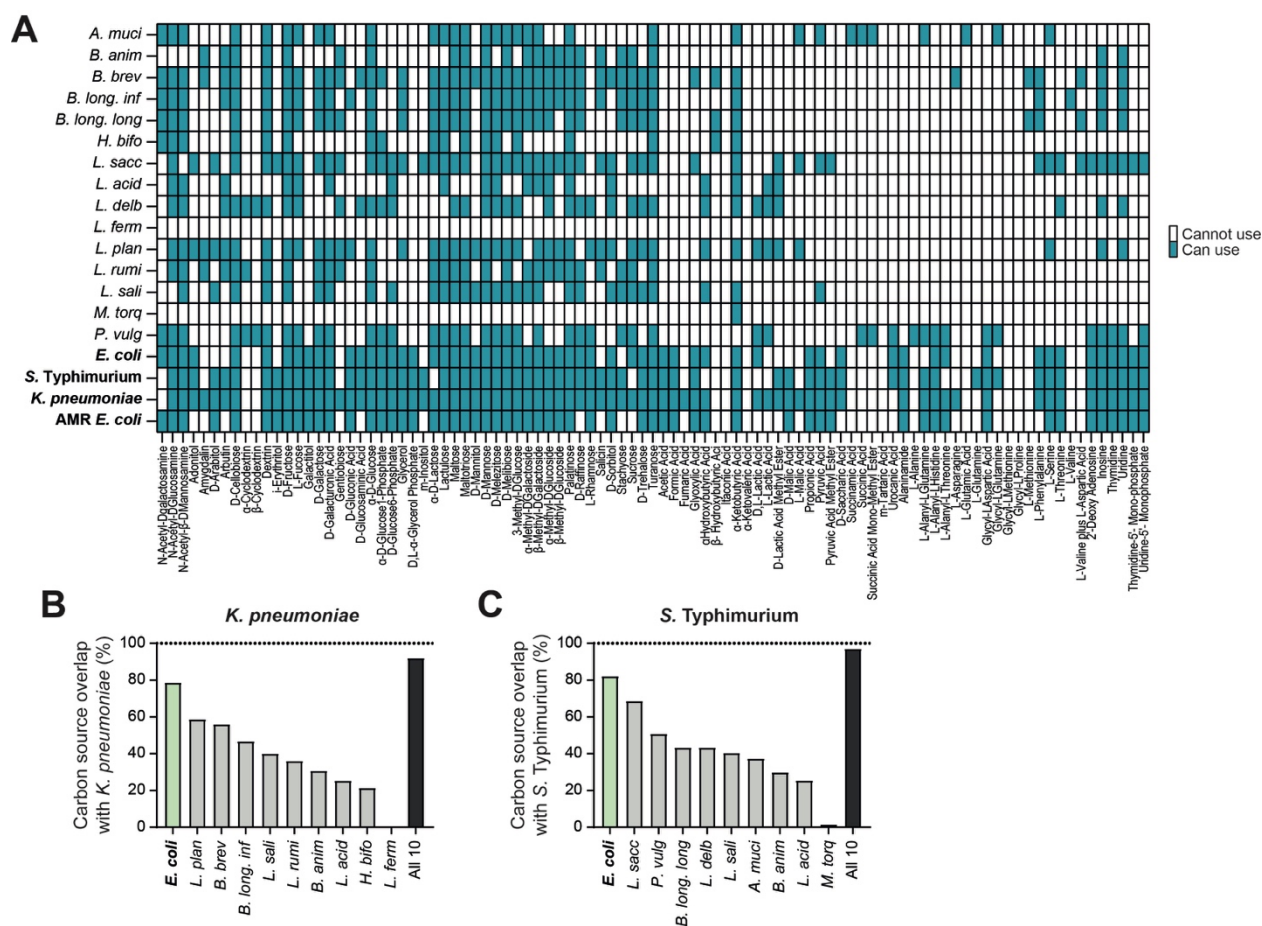
- 1-member
- 2-member
- 3-member
- 5-member
- 9-member
- 49-member
- *K. pneumoniae* or *S. Typhimurium* itself alone
- Media only

with *E. coli*

- 1-member
- 2-member
- 3-member
- 5-member
- 10-member
- 50-member

E**F**

1127 **Fig. S9.**
1128 **Protein family overlap between single strains or communities and the pathogen shows**
1129 **that both diversity and key members (*E. coli*) are important in explaining predicted**
1130 **colonization resistance. A-B)** As community diversity increases, protein family overlap with
1131 the pathogen increases. Results for *K. pneumoniae* shown in (A) and for *S. Typhimurium* in
1132 (B). Each circle represents a community (communities from Fig. 2C-D). Green circles depict
1133 communities containing *E. coli*, while black circles are communities without *E. coli*. Linear
1134 regression of log-transformed data: (A) $R^2=0.9350$, non-zero slope for *E. coli* communities (F
1135 test, $p<0.0001$). $R^2=0.9182$, non-zero slope for communities without *E. coli* (F test, $p<0.0001$).
1136 (B) $R^2=0.6825$, non-zero slope for *E. coli* communities (F test, $p<0.0001$). $R^2=0.7484$, non-
1137 zero slope for communities without *E. coli* (F test, $p<0.0001$). C-D) Bar chart showing the
1138 protein family overlap with the pathogen for the individual 10 best-ranked strains. Results for
1139 *K. pneumoniae* shown in (C) and for *S. Typhimurium* in (D). The bar for *E. coli* is shown in
1140 green and the other strains in grey. The predicted protein family overlap for all 10 strains is
1141 shown in dark grey. See Table S1 for species name abbreviations. E-F) As community cluster
1142 overlap with the pathogen increases, the pathogen abundance on day 2 of the extended
1143 competition decreases. Colored circles depict communities containing *E. coli*, while black
1144 circles represent communities without *E. coli* (data from Fig. 2C-D). Color or greyscale
1145 gradients indicate the diversity of the community. The red circles represent the isogenic
1146 wildtype pathogens. Results for *K. pneumoniae* shown in (E) and for *S. Typhimurium* in (F).
1147



1148

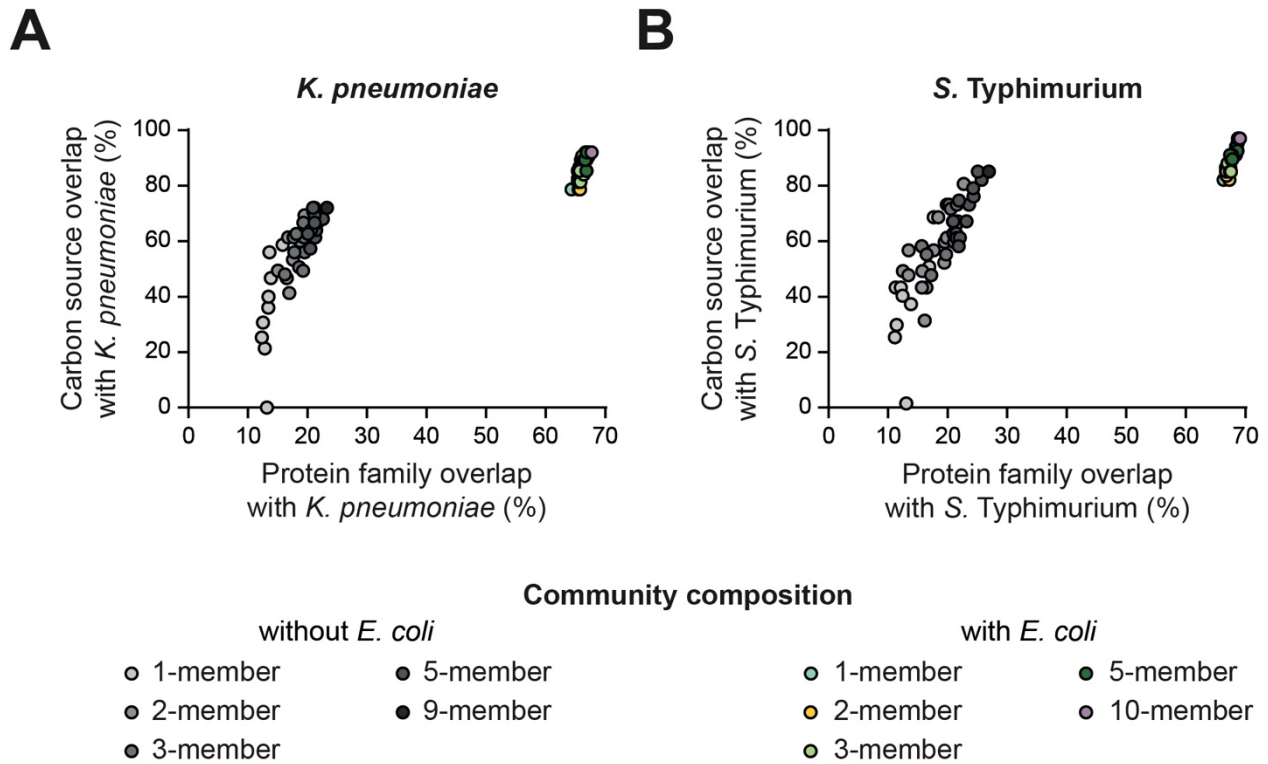
1149 **Fig. S10.**

1150 **Individual carbon source utilization profiles of the 10 best-ranked symbiont strains for**
 1151 ***K. pneumoniae* and *S. Typhimurium* (16 symbiont strains total) and their overlap with**
 1152 **the pathogens. (A)** The x-axis lists the 95 individual nutrients tested in the AN Biolog

1153 MicroPlates and the y-axis shows the 16 symbiont strains and the 3 pathogens (*K. pneumoniae*,
 1154 *S. Typhimurium*, AMR *E. coli*). The pathogens are highlighted in bold on the y-axis. Nutrients
 1155 shaded in blue could be used by a strain whereas those in white could not be used as defined

1156 by a threshold of background-subtracted Abs_{590nm}. Data used to apply thresholding is derived
 1157 from the median value of three biological replicates of AN Biolog measurements, coming from
 1158 three independent experiments. **B-C)** Bar charts showing carbon source utilization overlap (%)
 1159 of the 10 best ranked individual strains with the pathogens. Results for *K. pneumoniae* in **(B)**
 1160 and *S. Typhimurium* in **(C)**. *E. coli* is shown in green and the other individual strains in grey.
 1161 The predicted utilization of all 10 best-ranked symbionts together is shown in dark grey. The
 1162 percentage overlap with the pathogen is calculated as the proportion of the number of nutrients
 1163 able to be used by the pathogen that can also be used by a particular symbiont strain or
 1164 community. See **Table S1** for species name abbreviations.

1165

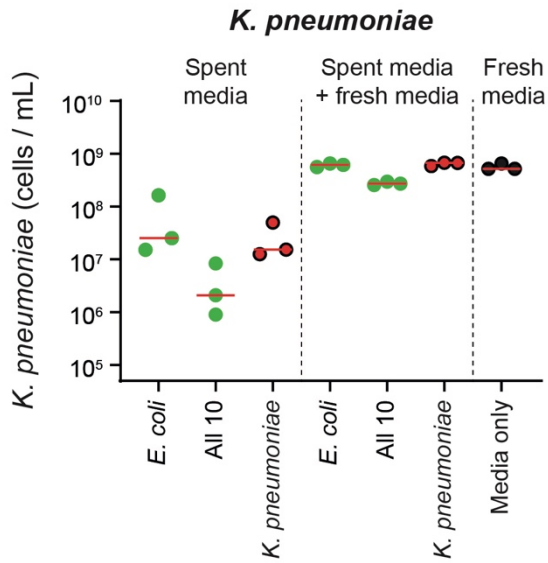
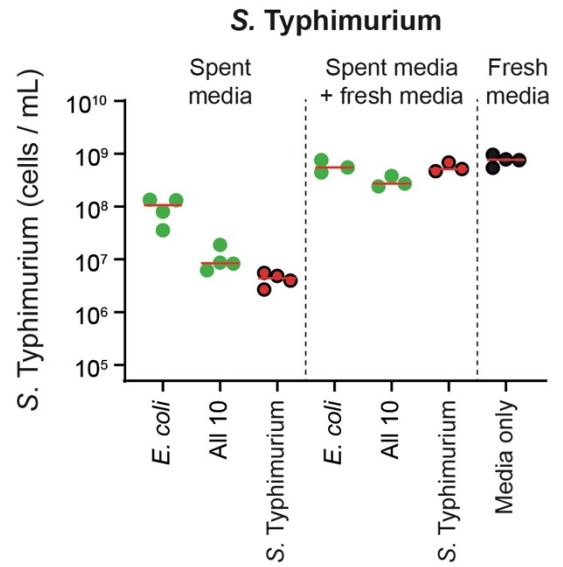


1166

1167 **Fig. S11.**

1168 **The protein family overlap and carbon source overlap prediction approaches are**
 1169 **positively correlated. A-B)** Correlation between protein cluster percentage overlap with the
 1170 pathogen and carbon source utilization percentage overlap with the pathogen. Results for *K.*
 1171 *pneumoniae* in **(A)** and *S. Typhimurium* in **(B)**. Communities shown in color contain *E. coli*
 1172 and those in black do not. Gradients of color or greyscale intensity show community diversity.
 1173 **(A)** $R^2=0.6119$, slope significantly different than 0 by an F test for communities with *E. coli*
 1174 ($p<0.0001$). $R^2=0.6838$, slope significantly different than 0 by an F test for communities
 1175 without *E. coli* ($p<0.0001$). **(B)** $R^2=0.8204$, slope significantly different than 0 by an F test for
 1176 communities with *E. coli* ($p<0.0001$). $R^2=0.7027$, slope significantly different than 0 by an F
 1177 test for communities without *E. coli* ($p<0.0001$). The communities are the same as those in **Fig.**
 1178 **2C-D**. Percentage overlap calculated as the proportion of shared carbon source use or shared
 1179 protein families with the pathogen. Values for communities calculated in an additive way based
 1180 on the profiles of individual strains. Each data point represents a community.

1181

A**B**

1182

1183 **Fig. S12.**

1184 **Spent media experiment.** Communities were assembled and grown for 96 hours and the
 1185 pathogen invaded into the spent media or re-supplemented spent media (half volume spent
 1186 media and half volume nutrient media). Pathogen density measured by flow cytometry 24 hours
 1187 after pathogen invasion (day 1). Results for *K. pneumoniae* shown in (A) and *S. Typhimurium*
 1188 in (B). *N*=3-4 biological replicates from different independent experiments per treatment.
 1189 Horizontal red lines show the median of the replicates.

1190

AMR *E. coli*

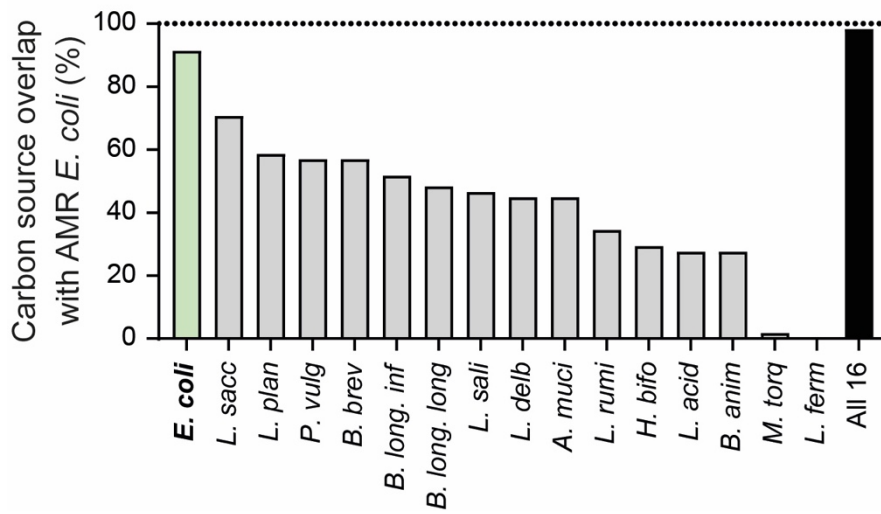


Fig. S13.

Carbon source utilization overlap with AMR *E. coli*. Bar chart showing carbon source utilization overlap (%) of the 16 best ranked individual strains (for *K. pneumoniae* and *S. Typhimurium*) with the AMR *E. coli* strain. The *E. coli* symbiont is shown in green and the other individual strains in grey. All 16 symbiont strains together are shown in black. The percentage overlap with the pathogen is calculated as the proportion of the number of nutrients that can be used by AMR *E. coli* that can also be used by a particular symbiont strain. Data used to apply thresholding is derived from the median value of 3 biological replicates of AN Biolog measurements, coming from three independent experiments.

Table S1.

Strains used in this study. *Relevant resistances only. Streptomycin=>50 ug/mL; carbenicillin=>50µg/mL; ampicillin=>100µg/mL; kanamycin=>50µg/mL; tetracycline=>50µg/mL. **According to European biosafety designation. *** Leibniz Institute DSMZ- German Collection of Microorganisms and Cell Cultures, Inhoffenstraße 7, 38124 Braunschwe, Science Campus Braunschweig-Süd, Germany. **** ATCC (American Type Culture Collection), 10801 University Boulevard, Manassas, Virginia 20110-2209, United States.

Strain	Abbrev.	Relevant genotype *	Internal ID	PATRIC ID	Collection ID	Hazard group**	100-strain screen	50-strain community	<i>K. pneumoniae</i> 10 best-ranked	<i>S. Typhimurium</i> 10 best-ranked	Source
<i>Actinomyces odontolyticus</i>			NT5039	411466.7	DSM43331	2	+				Nassos Typas
<i>Akkermansia muciniphila</i>	<i>A.muci</i>		F3	349741.6	DSM22959	1	+	+		+	DSMZ***
<i>Anaerostipes caccae</i>			F2	105841.35	DSM14662	1	+	+			DSMZ
<i>Bacteroides caccae</i>			B1	411901.7	DSM19024	2	+				DSMZ
<i>Bacteroides cellulosilyticus</i>			B2	537012.5	DSM14838	1	+	+			DSMZ
<i>Bacteroides clarus</i>			NT5052	762984.10	DSM22519	1	+	+			Nassos Typas

Strain	Abbrev.	Relevant genotype *	Internal ID	PATRIC ID	Collection ID	Hazard group**	100-strain screen	50-strain community	<i>K. pneumoniae</i> 10 best-ranked	<i>S. Typhimurium</i> 10 best-ranked	Source
<i>Bacteroides eggerthii</i>			B13	483216.6	DSM20697	2	+				DSMZ
<i>Bacteroides fragilis</i> enterotoxigenic 20656-2-1			NT5033	817.95	ATCC43860	2	+				Nassos Typas
<i>Bacteroides fragilis</i> 3_1_12			NT5057	457424.5	HM-20	2	+				Nassos Typas
<i>Bacteroides fragilis</i> CL07T12C05			NT5059	997883.3	HM-710	2	+				Nassos Typas
<i>Bacteroides fragilis</i> CL05T00C42			NT5060	997880.3	HM-711	2	+				Nassos Typas
<i>Bacteroides fragilis</i> CL05T12C13			NT5062	997881.3	HM-712	2	+				Nassos Typas
<i>Bacteroides fragilis</i> CL03T00C08			NT5063	997878.3	HM-713	2	+				Nassos Typas

Strain	Abbrev.	Relevant genotype *	Internal ID	PATRIC ID	Collection ID	Hazard group**	100-strain screen	50-strain community	<i>K. pneumoniae</i> 10 best-ranked	<i>S. Typhimurium</i> 10 best-ranked	Source
<i>Bacteroides fragilis</i> CL03T12C07			NT5061	997879.7	HM-714	2	+				Nassos Typas
<i>Bacteroides fragilis</i> nontoxigenic			B4	272559.17	DSM2151	2	+				DSMZ
<i>Bacteroides ovatus</i>			B6	411476.11	DSM1896	2	+				DSMZ
<i>Bacteroides stercoris</i> VPI B5-21			B8	46506.156 2	DSM19555	1	+	+			DSMZ
<i>Bacteroides stercoris</i> CC31F			NT5055	1073351.3	HM-1036	2	+				Nassos Typas
<i>Bacteroides thetaiotaomicron</i>			B9	226186.12	DSM2079	2	+				DSMZ
<i>Bacteroides uniformis</i>			B10	820.37	DSM6597	2	+				DSMZ
<i>Bacteroides uniformis</i> CL03T12C37			NT5066	997890.6	HM-716	2	+				Nassos Typas

Strain	Abbrev.	Relevant genotype *	Internal ID	PATRIC ID	Collection ID	Hazard group**	100-strain screen	50-strain community	<i>K. pneumoniae</i> 10 best-ranked	<i>S. Typhimurium</i> 10 best-ranked	Source
<i>Bacteroides xylanisolvens</i> XB1A			B12	657309.4	DSM18836	1	+	+			DSMZ
<i>Bacteroides xylanisolvens</i> CL03T12C04			NT5064	997892.50	DSM2079	2	+				Nassos Typas
<i>Bifidobacterium adolescentis</i>			NT5022	367928.6	DSM20083	1	+	+			Nassos Typas
<i>Bifidobacterium animalis</i>	<i>B. anim</i>		A2	555970.3	DSM10140	1	+	+	+	+	DSMZ
<i>Bifidobacterium animalis</i> subsp. lactis Bi-04			NT5043	580050.3		1	+				Nassos Typas
<i>Bifidobacterium animalis</i> subsp. lactis Bi-07			NT5044	742729.3	DGCC2908	1	+	+			Nassos Typas
<i>Bifidobacterium bifidum</i>			A1	500634.6	DSM20456	1	+	+			DSMZ
<i>Bifidobacterium breve</i>	<i>B. brev</i>		A3	518634.19	DSM20213	1	+	+	+		DSMZ
<i>Bifidobacterium longum</i> subsp. infantis	<i>B. long. inf</i>		A4	391904.8	DSM20088	1	+	+	+		DSMZ

Strain	Abbrev.	Relevant genotype *	Internal ID	PATRIC ID	Collection ID	Hazard group**	100-strain screen	50-strain community	<i>K. pneumoniae</i> 10 best-ranked	<i>S. Typhimurium</i> 10 best-ranked	Source
<i>Bifidobacterium longum</i> subsp. longum	<i>B. long.</i> long		A5	565042.3	DSM20219	1	+	+		+	DSMZ
<i>Blautia hansenii</i>			NT5005	537007.6	DSM20583	1	+	+			Nassos Typas
<i>Blautia hydrogenotrophica</i>			F4	476272.21	DSM10507	1	+	+			DSMZ
<i>Christensenella minuta</i>			F7	626937.8	DSM22607	1	+	+			DSMZ
<i>Clostridium difficile</i> 630			NT23006	272563.8	DSM27543	2	+				Nassos Typas
<i>Clostridium leptum</i>			F12	428125.8	DSM753	1	+	+			DSMZ
<i>Clostridium perfringens</i>			NT5031	195103.10	DSM756	2	+				Nassos Typas
<i>Clostridium perfringens</i>			NT5032	451754.18	DSM11782	2	+				Nassos Typas
<i>Collinsella aerofaciens</i>			A6	411903.6	DSM3979	2	+				DSMZ

Strain	Abbrev.	Relevant genotype *	Internal ID	PATRIC ID	Collection ID	Hazard group**	100-strain screen	50-strain community	<i>K. pneumoniae</i> 10 best-ranked	<i>S. Typhimurium</i> 10 best-ranked	Source
<i>Coprococcus comes</i>			NT5048	470146.3	ATCC27758	1	+	+			Nassos Typas
<i>Dorea formicigenerans</i>			NT5076	411461.20	DSM3992	1	+	+			Nassos Typas
<i>Dorea longicatena</i>			F13	411462.6	DSM13814	1	+	+			DSMZ
<i>Eggerthella lenta</i>			NT5024	479437.5	DSM2243	2	+				Nassos Typas
<i>Enterocloster bolteae</i>			NT5026	208479.10	DSM15670	1	+	+			Nassos Typas
<i>Erysipelatoclostridium ramosum</i>			NT5006	445974.19	DSM1402	2	+				Nassos Typas
AMR <i>Escherichia coli</i>		Wildtype (Ampicilin)	19Y000018		-	2					Nottingham University Hospital Pathogen Bank
<i>Escherichia coli</i> ED1a			NT5078	585397.9		1	+				Nassos Typas
<i>Escherichia coli</i> HS			e-OPC-323	331112.6		1	+				(34)

Strain	Abbrev.	Relevant genotype *	Internal ID	PATRIC ID	Collection ID	Hazard group**	100-strain screen	50-strain community	<i>K. pneumoniae</i> 10 best-ranked	<i>S. Typhimurium</i> 10 best-ranked	Source
<i>Escherichia coli</i> IAI1	<i>E. coli</i>		NT5077	585034.5		1	+	+	+	+	Nassos Typas
<i>Escherichia coli</i> IAI1	<i>E. coli</i> Δ gatABC	Δ gatABC	eOPC-364			1					This study
<i>Escherichia coli</i> JKE201	+pOPC-231		eOPC-362			1					This study
<i>Escherichia coli</i> JKe201	+pOPC-232		eOPC-363			1					This study
<i>Escherichia coli</i> MG1655			e-OPC-292	511145.12		1	+				(35)
<i>Escherichia coli</i> Z1269			Z1269		-	1					(33)
<i>Escherichia coli</i> Z1331			Z1331		-	1					(33)
<i>Eubacterium rectale</i>			NT5009	657318.12	DSM17629	1	+	+			Nassos Typas
<i>Eubacterium siraeum</i>			NT5040	428128.19	DSM15702	1	+	+			Nassos Typas
<i>Faecalibacterium prausnitzii</i>			F25	411483.3	DSM17677	1		+			DSMZ

Strain	Abbrev.	Relevant genotype *	Internal ID	PATRIC ID	Collection ID	Hazard group**	100-strain screen	50-strain community	<i>K. pneumoniae</i> 10 best-ranked	<i>S. Typhimurium</i> 10 best-ranked	Source
<i>Fusobacterium nucleatum</i> CTI-01			NT24006	1204474.3		2	+				Nassos Typas
<i>Fusobacterium nucleatum</i> MJR7757B			NT24015	851.8		2	+				Nassos Typas
<i>Fusobacterium nucleatum</i> subsp. <i>nucleatum</i>			NT5025	190304.8	DSM15643	2	+				Nassos Typas
<i>Fusobacterium nucleatum</i> subsp. <i>vincentii</i>			NT24005	155615.5	DSM19508	2	+				Nassos Typas
<i>Fusobacterium nucleatum</i> subsp. <i>vincentii</i>			NT5030	209882.4	DSM19507	2	+				Nassos Typas
<i>Fusobacterium periodonticum</i> 1_A_54/D10			NT24011	546275.3	ATCC33693	1	+	+			Nassos Typas
<i>Fusobacterium periodonticum</i> 2_1_31			NT24012	469599.3		2	+				Nassos Typas
<i>Gemella morbillorum</i>			NT24013	562982.3		2	+				Nassos Typas
<i>Holdemanella biformis</i>	<i>H. bifo</i>		F15	518637.5	DSM3989	1	+	+	+		DSMZ

Strain	Abbrev.	Relevant genotype *	Internal ID	PATRIC ID	Collection ID	Hazard group**	100-strain screen	50-strain community	<i>K. pneumoniae</i> 10 best-ranked	<i>S. Typhimurium</i> 10 best-ranked	Source
<i>Intestinibacter bartletti</i>			NT5086	261299.118	DSM16795	1	+				Nassos Typas
<i>Klebsiella pneumoniae</i>			K1	272620.9	ATCC 700721	2	+				Modernising Medical Microbiology, Nuffield Department of Medicine
<i>Klebsiella pneumoniae</i> subsp. <i>pneumoniae</i>		Wildtype (Carbenicillin)	bFS-26	1162296.3	DSM 30104	2	+				DSMZ
<i>Klebsiella pneumoniae</i> subsp. <i>pneumoniae</i>		+ pRSJ-p _{npII} ::ilux	bFS-29		DSM 30104	2					This study
<i>Klebsiella pneumoniae</i> subsp. <i>pneumoniae</i>		+pBC11	bFS-34		DSM 30104	2					This study
<i>Lachnoclostridium symbiosum</i> WAL-14163			NT24007	742740.3		2	+				Nassos Typas

Strain	Abbrev.	Relevant genotype *	Internal ID	PATRIC ID	Collection ID	Hazard group**	100-strain screen	50-strain community	<i>K. pneumoniae</i> 10 best-ranked	<i>S. Typhimurium</i> 10 best-ranked	Source
<i>Lachnoclostridium symbiosum</i> WAL-14673			NT24014	742741.3		2	+				Nassos Typas
<i>Lachnoclostridium hylemonae</i>			NT27002	553973.19	DSM15053	1	+	+			Nassos Typas
<i>Lachnoclostridium scindens</i>			F9	411468.41	DSM5676	1	+	+			DSMZ
<i>Lachnoclostridium symbiosum</i>			F8	411472.5	DSM934	2	+				DSMZ
<i>Lacrimispora saccharolytica</i>	<i>L. sacc</i>		NT5037	610130.3	DSM2544	1	+	+		+	Nassos Typas
<i>Lacticaseibacillus casei</i>			F16	219334.4	DSM20011	1	+	+			DSMZ
<i>Lacticaseibacillus paracasei</i>			NT5042	1226298.3	ATCCSD5 275	1	+	+			Nassos Typas
<i>Lactiplantibacillus plantarum</i> JDM1	<i>L. plan</i>		F14	644042.3	-	1	+	+	+		Department of Food and Nutritional Sciences, University of Reading

Strain	Abbrev.	Relevant genotype *	Internal ID	PATRIC ID	Collection ID	Hazard group**	100-strain screen	50-strain community	<i>K. pneumoniae</i> 10 best-ranked	<i>S. Typhimurium</i> 10 best-ranked	Source
<i>Lactobacillus acidophilus</i>	<i>L. acid</i>		NT5041	272621.13	ATCC700936	1	+	+	+	+	Nassos Typas
<i>Lactobacillus delbrueckii</i> subsp. <i>Delbrueckii</i>	<i>L. delb</i>		NT14075	1423823.4	DSM20074	1	+	+		+	Nassos Typas
<i>Lactobacillus gasseri</i>			F18	324831.13	DSM20243	1	+	+			DSMZ
<i>Ligilactobacillus ruminis</i>	<i>L. rumi</i>		F17	1423798.5	DSM20403	1	+	+	+		DSMZ
<i>Ligilactobacillus salivarius</i>	<i>L. sali</i>		NT14072	1423799.3	DSM20555	1	+	+	+	+	Nassos Typas
<i>Limosilactobacillus fermentum</i>	<i>L. ferm</i>		NT14076	1613.547	DSM20052	1	+	+	+		Nassos Typas
<i>Mediterraneibacter gnavus</i>			NT5046	411470.47	ATCC29149	1	+	+			Nassos Typas
<i>Mediterraneibacter torques</i>	<i>M. torq</i>		NT5047	411460.6	ATCC27756	1	+	+		+	Nassos Typas
<i>Odoribacter splanchnicus</i>			NT5081	709991.142	DSM20712	2	+				Nassos Typas

Strain	Abbrev.	Relevant genotype *	Internal ID	PATRIC ID	Collection ID	Hazard group**	100-strain screen	50-strain community	<i>K. pneumoniae</i> 10 best-ranked	<i>S. Typhimurium</i> 10 best-ranked	Source
<i>Parabacteroides distasonis</i>			NT5074	435591.48	DSM20701	2	+				Nassos Typas
<i>Parabacteroides merdae</i>			NT5071	411477.88	DSM19495	1	+				Nassos Typas
<i>Peptostreptococcus stomatis</i>			NT24002	596315.3	DSM17678	2	+				Nassos Typas
<i>Phocaeicola coprocola</i>			B3	470145.69	DSM17136	1	+	+			DSMZ
<i>Phocaeicola dorei</i>			NT5049	357276.10 35	DSM17855	1	+	+			Nassos Typas
<i>Phocaeicola massiliensis</i>			B5	1121098.3	DSM17679	1	+	+			DSMZ
<i>Phocaeicola vulgatus</i>	<i>P. vulg</i>		B11	435590.9	DSM1447	1	+	+		+	DSMZ
<i>Phocaeicola vulgatus</i> CL09T03C04			NT5056	997891.3		1	+				Nassos Typas
<i>Prevotella buccae</i>			B14	873513.3	DSM19025	2	+				DSMZ

Strain	Abbrev.	Relevant genotype *	Internal ID	PATRIC ID	Collection ID	Hazard group**	100-strain screen	50-strain community	<i>K. pneumoniae</i> 10 best-ranked	<i>S. Typhimurium</i> 10 best-ranked	Source
<i>Prevotella copri</i>			B15	537011.439	DSM18205	1	+	+			DSMZ
<i>Roseburia faecis</i>			F24	301302.4	DSM16840	1	+	+			DSMZ
<i>Roseburia hominis</i>			F22	585394.18	DSM16839	1	+	+			DSMZ
<i>Roseburia intestinalis</i>			NT5011	536231.75	DSM14610	1	+	+			Nassos Typas
<i>Roseburia inulinivorans</i>			NT5012	622312.48	DSM16841	1	+	+			Nassos Typas
<i>Salmonella enterica</i> Typhimurium SL1344		Wildtype (Streptomycin)	SB300	216597.6	DSM24522	2	+				(57)
<i>Salmonella enterica</i> Typhimurium SL1344		+ pRSJ-p _{npII} ::ilux	sOPC-406		DSM24522	2					This study
<i>Salmonella enterica</i> Typhimurium SL1344		+pBC11	sOPC-404		DSM24522	2					This study

Strain	Abbrev.	Relevant genotype *	Internal ID	PATRIC ID	Collection ID	Hazard group**	100-strain screen	50-strain community	<i>K. pneumoniae</i> 10 best-ranked	<i>S. Typhimurium</i> 10 best-ranked	Source
<i>Salmonella enterica</i> Typhimurium SL1344		Avirulent	M2702		DSM24522	2					(72)
<i>Salmonella enterica</i> Typhimurium SL1344		<i>hisG</i> prototroph (Streptomycin)	EB199		DSM24522	2					This study
<i>Salmonella enterica</i> Typhimurium SL1344		$\Delta gatABC$ (Streptomycin)	sOPC-463		DSM24522	2					This study
<i>Salmonella enterica</i> Typhimurium SL1344		$\Delta gatABC$ +pBC11	EB149		DSM24522	2					This study
<i>Staphylococcus epidermis</i>			bOPC-105	176280.85	DSM1798	2	+				ATCC****
<i>Streptococcus parasanguinis</i>			NT5072	760570.3	DSM6778	2	+				Nassos Typas
<i>Streptococcus salivarius</i>			NT5038	1304.1829	DSM20560	2	+				Nassos Typas

Strain	Abbrev.	Relevant genotype *	Internal ID	PATRIC ID	Collection ID	Hazard group**	100-strain screen	50-strain community	<i>K. pneumoniae</i> 10 best-ranked	<i>S. Typhimurium</i> 10 best-ranked	Source
<i>Veillonella parvula</i>			NT5017	479436.6	DSM2008	2	+				Nassos Typas

Table S2.

Plasmids used in this study. *Relevant resistances only. Streptomycin=>50 ug/mL; carbenicillin=>50µg/mL; ampicillin=>100µg/mL; kanamycin=>50µg/mL; tetracycline=>50µg/mL.

Plasmid name	Relevant genotype	Resistance*	Source
pRSJ-p _{nptII} ::ilux	<i>luxCDBAE-fp</i> expression	Tetracycline	(61)
pBC11	YPet expression	Kanamycin	(64)
pOPC-231	<i>SV-aphT-tetR-sceI-sacB-STm-ΔgatABC</i>	Kanamycin	This study
pOPC-232	<i>SV-aphT-tetR-sceI-sacB-EcIAI-ΔgatABC</i>	Kanamycin	This study

Table S3.

Primers used in this study.

Primer name	Sequence	Purpose	Source
oOPC-953	AGAGTTTGATCCTGGCTCAG	16S sequencing (27F)	(73)
oOPC-954	TACGGYTACCTTGTTACGACTT	16S sequencing (1492R)	(73)
g-Bifid-F	5'-CTCCTGGAAACGGGTGG-3'	16S sequencing for Bifidobacteria	(74)
g-Bifid-R	5'-GGTGTCTCTCCCGATATCTACA-3'		(74)
oOPC-975	CCCAGTCTCGAGGTCGACGGTATCGATAAGCTTGA TATCGAATTCaatcgcgttctgtaacagg	amplify 700 upstream <i>gatABC</i> for deletion - STm SL1344	This study
oOPC-976	taaaattaagagcgcattgaaatagttggctcataaattctccattattcagg		This study
oOPC-977	aatttatgagccaactatttcaaatcgctcttaatttaggggag	amplify 700 downstream <i>gatABC</i> for deletion - STm	This study
oOPC-978	CTGGAGCTCCACCGCGGTGGCGGCCGCTCTAGAAC TAGTGGATCCtcccggctattacaggtatgcgttgccg		This study
oOPC-979	agtcgatgctgcacgtacgc	check <i>gatABC</i> deletion - STm	This study
oOPC-980	atgtcggacaacgcggctctg		This study
oOPC-981	CCCAGTCTCGAGGTCGACGGTATCGATAAGCTTGA TATCGAATTCtactgttaaatggttgcacgcacc	amplify 700 upstream <i>gatABC</i> for deletion - <i>E.coli</i> IA11	This study
oOPC-982	ggtatatgactaacctgttgttctcgcagaataattttacctgaggg		This study
oOPC-983	aaaaattattctgcgagaacaacaggttagtcatataccgtcctattccg	amplify 700 downstream <i>gatABC</i> for deletion - <i>E.coli</i> IA11	This study
oOPC-984	CTGGAGCTCCACCGCGGTGGCGGCCGCTCTAGAAC TAGTGGATCCttacgtacgcatcaaaagcctttattgcc		This study
oOPC-985	aaacgctctgcatttgccgc	check <i>gatABC</i> deletion - <i>E.coli</i> IA11	This study
oOPC-986	cccatgttgaagatgccgc		This study

Table S4.

Species compositions of communities used for *in vitro* experiments with *K. pneumoniae* DSM 30104. *Communities that were additionally selected to contain *E. coli* IAI1, but otherwise were selected at random.

Community ID	Community members	No. replicates	Median day 2 pathogen density (cells/mL)
No commensals	N/A	15	1.84E+09
KTS1	A3	5	9.45E+08
KTS2	F15	3	1.11E+09
KTS3	F17	3	1.19E+09
KTS4	A4	3	1.29E+09
KTS5	NT5077	3	1.10E+08
KTS6	NT5041	3	1.12E+09
KTS7	A2	3	1.28E+09
KTS8	F14	3	1.21E+09
KTS9	NT14076	3	1.68E+09
KTS10	NT14072	3	1.53E+09
KTD1	A4, NT5041	3	1.33E+09
KTD2	NT5041, F14	3	1.29E+09
KTD3	A3, NT5077	4	4.58E+06
KTD4	F15, F14	3	1.40E+09
KTD5	F15, A2	3	1.83E+09
KTD6	A2, F14	3	1.70E+09
KTD7	F17, NT14072	3	1.59E+09
KTD8	NT5077, NT14076	4	1.28E+08
KTD9	A3, F14	3	5.96E+08
KTD10*	NT5077, F14	3	1.82E+07
KTD11*	F15, NT5077	3	1.09E+08
KTD12*	F17, NT5077	3	3.42E+07

Community ID	Community members	No. replicates	Median day 2 pathogen density (cells/mL)
KTD13*	A4, NT5077	3	7.44E+07
KTD14*	NT5077, NT5041	3	1.55E+07
KTD15*	NT5077, A2	3	3.84E+07
KTD16*	NT5077, NT14072	3	2.90E+07
KTD17*	NT5041, A2	3	1.81E+09
KTT1	A3, F15, NT5041	3	3.30E+08
KTT2	A3, F15, A2	3	7.44E+08
KTT3	A2, NT14076, NT14072	3	6.56E+08
KTT4	F17, NT5077, NT14072	3	1.12E+07
KTT5	NT5041, NT14076, NT14072	3	7.11E+08
KTT6	F17, NT5077, A2	3	2.52E+07
KTT7	F17, A4, NT14076	3	1.07E+09
KTT8	A3, F15, F17	4	5.03E+08
KTT9	A3, NT5041, A2	3	7.59E+08
KTT10	A3, A4, NT5041	3	6.13E+08
KTT11	A2, F14, NT14072	3	1.19E+09
KTT12	A4, NT5041, F14	3	9.36E+08
KTT13	F15, F14, NT14072	3	1.13E+09
KTT14	A3, NT5077, F14	3	3.81E+05
KTT15	A3, F17, A2	3	5.07E+08
KTT16	NT5077, F14, NT14072	3	1.72E+07
KTT17	NT5077, NT14076, NT14072	3	1.43E+07
KTT23*	A3, F15, NT5077	2	8.73E+05
KTT24*	A4, NT5077, NT14072	3	1.29E+07
KTT25*	A3, NT5077, A2	3	6.53E+05
KTT26*	NT5077, NT5041, NT14072	3	6.20E+06
KTP1	A3, F15, F17, NT5041, NT14076	4	4.77E+08
KTP2	A3, F15, NT5041, A2, NT14072	4	2.98E+08

Community ID	Community members	No. replicates	Median day 2 pathogen density (cells/mL)
KTP3	NT5077, A2, F14, NT14076, NT14072	4	1.66E+07
KTP4	F17, NT5077, NT5041, A2, NT14072	4	2.42E+07
KTP5	A3, F15, NT5041, NT14076, NT14072	4	3.63E+08
KTP6	A3, F15, F17, A4, A2	4	5.33E+08
KTP7	F17, A4, NT5077, A2, NT14076	4	2.63E+07
KTP8	A3, F15, F17, NT5077, NT5041	4	1.25E+06
KTP9	A3, A4, NT5041, A2, F14	4	1.85E+08
KTP10	A3, A4, NT5041, F14, NT14072	4	1.99E+08
KTP11	F15, NT5041, A2, F14, NT14072	4	1.19E+09
KTP12	F17, NT5041, A2, F14, NT14076	4	9.19E+08
KTP13	F15, A4, F14, NT14076, NT14072	4	9.89E+08
KTP14	A3, A4, A2, F14, NT14076	4	6.60E+08
KTP15	F17, A4, F14, NT14076, NT14072	4	1.28E+09
KTP16	A3, F17, A4, F14, NT14072	4	2.95E+08
KTP17	A3, A4, A2, NT14076, NT14072	4	2.67E+08
KTP18*	F15, NT5077, NT5041, A2, F14	3	2.72E+06
KTP19*	F17, A4, NT5077, F14, NT14076	3	1.28E+07
KTP20*	A3, NT5077, NT5041, A2, NT14076	3	2.82E+05
KTP21*	A3, F15, NT5077, NT5041, F14	3	3.26E+05
KTP22*	A3, F17, NT5077, NT5041, F14	3	3.08E+05
KALLTOP	A3, F15, F17, A4, NT5077, NT5041, A2, F14, NT14076, NT14072	11	6.17E+05

Table S5.

Species compositions of communities used for *in vitro* experiments with *S. enterica* serovar Typhimurium SL1344. *Communities that were additionally selected to contain *E. coli* IAI1, but otherwise were selected at random.

Community ID	Community members	No. replicates	Median day 2 pathogen density (cells/mL)
No commensals	N/A	11	1.38E+09
STS1	A2	3	7.64E+08
STS2	NT5037	3	6.29E+08
STS3	NT14075	3	8.71E+08
STS4	F3	3	9.55E+08
STS5	NT5041	3	9.26E+08
STS6	A5	3	8.69E+08
STS7	NT5077	5	4.46E+08
STS8	B11	4	8.14E+08
STS9	NT5047	3	1.18E+09
STS10	NT14072	3	1.08E+09
STD1	NT5037, B11	3	6.04E+08
STD2	NT5077, NT5047	3	3.60E+08
STD3	NT5041, B11	3	7.16E+08
STD4	A5, NT5047	3	9.19E+08
STD5	NT14075, NT5077	3	3.98E+08
STD6	NT5037, NT14072	3	6.30E+08
STD7	B11, NT5047	3	7.64E+08
STD8	NT14075, NT14072	3	9.23E+08
STD9	NT5037, NT5047	3	7.74E+08
STD10	NT14075, NT5047	3	9.25E+08
STD11	NT14075, NT5041	3	9.62E+08
STD12	NT5041, NT14072	3	9.98E+08

Community ID	Community members	No. replicates	Median day 2 pathogen density (cells/mL)
STD13	A2, NT14072	3	1.06E+09
STD14	A2, NT5047	3	8.40E+08
STD15	B11, NT14072	3	7.79E+08
STD16	NT14075, F3	3	1.07E+09
STD17*	A2, NT5077	3	3.36E+08
STD18*	NT5037, NT5077	4	5.73E+07
STD19*	F3, NT5077	3	3.23E+08
STD20*	NT5041, NT5077	3	3.11E+08
STD21*	A5, NT5077	3	3.52E+08
STD22*	NT5077, B11	7	3.94E+07
STD23*	NT5077, NT14072	3	4.14E+08
STT1	A2, NT14075, A5	3	9.50E+08
STT2	NT14075, F3, B11	3	1.00E+09
STT3	F3, NT5041, NT5077	3	5.51E+08
STT4	A2, A5, NT14072	3	1.15E+09
STT5	A2, NT5037, A5	3	9.38E+08
STT6	NT5037, NT5077, NT14072	3	1.25E+08
STT7	F3, NT5041, A5	3	1.26E+09
STT8	NT5037, A5, NT5047	3	1.05E+09
STT9	NT5037, F3, NT5077	3	1.44E+08
STT10	NT5037, A5, NT14072	3	9.17E+08
STT11	NT14075, B11, NT5047	3	9.20E+08
STT12	A2, NT14075, B11	3	1.10E+09
STT13	A5, B11, NT14072	3	9.89E+08
STT14	NT5041, NT5047, NT14072	3	1.26E+09
STT15	A5, B11, NT5047	3	1.25E+09
STT16	A2, F3, B11	3	1.22E+09
STT17*	NT5037, NT5077, B11	5	2.23E+07

Community ID	Community members	No. replicates	Median day 2 pathogen density (cells/mL)
STT18*	A2, NT14075, NT5077	3	3.75E+08
STT19*	NT5041, NT5077, NT5047	3	3.80E+08
STT20*	NT5037, NT5077, NT5047	3	6.17E+07
STT21*	F3, NT5077, NT5047	3	3.79E+08
STT22*	NT14075, NT5077, B11	3	3.87E+07
STP1	NT14075, F3, NT5041, NT5047, NT14072	4	1.19E+09
STP2	A2, NT5037, NT14075, NT5077, NT14072	4	1.65E+08
STP3	NT14075, F3, A5, B11, NT14072	4	9.01E+08
STP4	A2, F3, A5, B11, NT5047	4	1.05E+09
STP5	F3, NT5041, A5, NT5077, B11	4	4.53E+07
STP6	NT5037, F3, B11, NT5047, NT14072	4	6.69E+08
STP7	NT14075, F3, NT5041, A5, NT5047	4	1.09E+09
STP8	A2, NT5037, F3, NT5041, NT5047	4	1.07E+09
STP9	NT5037, NT14075, A5, B11, NT14072	4	9.40E+08
STP10	A2, F3, NT5041, A5, NT5047	4	1.40E+09
STP11	A2, NT5037, A5, NT5077, B11	4	2.55E+07
STP12	NT5037, A5, NT5077, NT5047, NT14072	4	1.46E+08
STP13	A2, NT14075, A5, B11, NT14072	4	8.71E+08
STP14	F3, NT5041, NT5077, NT5047, NT14072	4	4.59E+08
STP15	A2, NT5037, NT14075, F3, A5	4	1.06E+09
STP16	A2, NT14075, F3, A5, NT14072	4	1.19E+09
STP17*	NT5041, A5, NT5077, B11, NT14072	3	2.01E+07
STP18*	NT5037, NT5041, A5, NT5077, B11	3	9.83E+06
STP19*	NT14075, F3, A5, NT5077, NT14072	3	4.38E+08
STP20*	A2, F3, A5, NT5077, B11	3	1.83E+07
SALLTOP	A2, NT5037, NT14075, F3, NT5041, A5, NT5077, B11, NT5047, NT14072	11	1.76E+07

Table S6.

Species compositions of communities used for gnotobiotic mouse experiments.

Pathogen gavaged	No. symbionts in community	Community members	<i>E. coli</i> IAI1 present	No. replicates	Median pathogen fecal density 24 hours p.i. (CFU/g)
<i>K. pneumoniae</i>	0	N/A	No	7	4.0375e+09
<i>K. pneumoniae</i>	1	NT5077	Yes	7	2.28846e+08
<i>K. pneumoniae</i>	5	KTP8 (see Table S4)	Yes	8	4.35148e+07
<i>K. pneumoniae</i>	10	KALLTOP (see Table S4)	Yes	7	4.07019e+07
<i>K. pneumoniae</i>	50	See Table S1	Yes	7	134667
<i>K. pneumoniae</i>	9	KALLTOP minus NT5077	No	7	4.4e+08
<i>K. pneumoniae</i>	49	50 minus NT5077	No	7	2.32e+07
<i>S. Typhimurium</i>	0	N/A	No	7	7.89e+08
<i>S. Typhimurium</i>	1	NT5077	Yes	7	9.01408e+07
<i>S. Typhimurium</i>	5	STP11 (see Table S5)	Yes	8	5.68115e+07
<i>S. Typhimurium</i>	10	SALLTOP (see Table S5)	Yes	7	4.1e+07
<i>S. Typhimurium</i>	50	See Table S1	Yes	7	521000
<i>S. Typhimurium</i>	9	SALLTOP minus NT5077	No	8	6.91e+08
<i>S. Typhimurium</i>	49	50 minus NT5077	No	7	2.15e+07

Table S7.

Species compositions of communities used for prediction experiments with the AMR *E. coli* strain 19Y000018.

Community ID	Community members	No. replicates	Median day 2 pathogen density (CFU/mL)
No commensals	N/A	5	4.96E+08
Best 2 Biolog	NT5077, NT5037	5	1.00E+07
Worst 2 Biolog	NT5077, A2	5	3.12E+08
Best 3 Biolog	NT5077, B11, NT5037	5	1.56E+06
Worst 3 Biolog	NT5077, F17, NT5041	5	2.64E+08
Best 5 Biolog	NT5077, NT5037, NT14075, NT5041, B11	5	2.48E+06
Worst 5 Biolog	NT5077, NT14075, A5, A3, F17	5	4.64E+06
Best 2 protein family	NT5077, NT5026	5	1.80E+07
Worst 2 protein family	NT5077, F3	5	2.48E+08
Best 3 protein family	NT5077, NT5026, F2	5	1.60E+07
Worst 3 protein family	NT5077, A2, NT5044	5	2.24E+08
Best 5 protein family	NT5077, NT5026, F2, NT5049, NT24011	5	2.80E+06
Worst 5 protein family	NT5077, NT14072, NT5041, F24, NT5040	5	8.16E+06
Best 10 protein family	NT5077, F2, NT14076, NT5026, NT5049, NT5047, F25, NT24011, NT5037, NT5012	5	1.60E+06
Worst 10 protein family	NT5077, F17, NT5041, NT5076, NT5048, A1, F15, A2, NT5009, NT5044	5	3.40E+06
Best 5 protein family #2	NT5077, NT5026, NT24011, NT5037, NT5052	5	4.00E+06

Community ID	Community members	No. replicates	Median day 2 pathogen density (CFU/mL)
Best 5 protein family #3	NT5077, NT5026, NT24011, NT5037, NT5049	5	2.02E+06
Best 5 protein family #4	NT5077, F2, NT24011, NT5037, NT5052	5	5.52E+06
Best 5 protein family #5	NT5077, F2, NT5026, F16, NT5049	5	2.48E+06
Worst 5 protein family #2	NT5077, F17, F15, A2, NT5044	5	3.00E+08
Worst 5 protein family #3	NT5077, NT5048, F15, A2, NT5044	5	2.32E+08
Worst 5 protein family #4	NT5077, NT14072, NT5040, A2, NT5044	5	3.20E+08
Worst 5 protein family #5	NT5077, F17, A1, A2, NT5044	5	2.80E+08

Supplementary references

72. B. Periaswamy et al., *Live attenuated S. Typhimurium vaccine with improved safety in immuno-compromised mice. PLoS One* 7, e45433 (2012).
73. J. S. Johnson et al., *Evaluation of 16S rRNA gene sequencing for species and strain-level microbiome analysis. Nat Commun* 10, 5029 (2019).
74. T. Matsuki et al., *Development of 16S rRNA-gene-targeted group-specific primers for the detection and identification of predominant bacteria in human feces. Appl Environ Microbiol* 68, 5445-5451 (2002).